Vital Sign Estimation through Doppler Radar

by

Hitesh Devshi Khunti

A Thesis Presented in Partial Fulfillment
of the Requirements for the Degree
Master of Science

Approved July 2013 by the
Graduate Supervisory Committee:

Sayfe Kiaei, Chair
Bertan Bakkaloglu
Daniel Bliss
Jennifer Kitchen

ARIZONA STATE UNIVERSITY

August 2013

ABSTRACT

Doppler radar can be used to measure respiration and heart rate without contact and through obstacles. In this work, a Doppler radar architecture at 2.4 GHz and a new signal processing algorithm to estimate the respiration and heart rate are presented. The received signal is dominated by the transceiver noise, LO phase noise and clutter which reduces the signal-to-noise ratio of the desired signal. The proposed architecture and algorithm are used to mitigate these issues and obtain an accurate estimate of the heart and respiration rate. Quadrature low-IF transceiver architecture is adopted to resolve null point problem as well as avoid 1/f noise and DC offset due to mixer-LO coupling. Adaptive clutter cancellation algorithm is used to enhance receiver sensitivity coupled with a novel Pattern Search in Noise Subspace (PSNS) algorithm is used to estimate respiration and heart rate. PSNS is a modified MUSIC algorithm which uses the phase noise to enhance Doppler shift detection. A prototype system was implemented using off-the-shelf TI and RFMD transceiver and tests were conduct with eight individuals. The measured results shows accurate estimate of the cardio pulmonary signals in low-SNR conditions and have been tested up to a distance of 6 meters.

DEDICATION

To my parents for providing me the luxury and freedom to explore my interest and career further.

ACKNOWLEDGMENTS

I am grateful to Prof. Kiaei for providing me an opportunity to work on this project. I thank him for his support, enthusiasm and for being patient with me. I am grateful for his constant encouragement and belief in me during the lows of the project.

I would also like to thank Prof. Bertan, Prof. Bliss and Prof. Kitchen for their generous advice and valuable critique on my work.

I thank my colleagues James and Michael for helping me with the hardware and also for being my companions to lunches which would have been lonely without them.

I thank my friends: Mohit Shah, Prasanna Sattigeri and Vinayak T.V for the brain storming sessions over evening coffees during which I was introduced to many exciting ideas and concepts in machine learning restoring my scientific vigor. I also thank them for the late night jamming sessions which rejuvenated our spirits.

I also thank Evie Holmgren and Margaret Creedon for helping me through procurement of components and administrative end of the research. Without whom my work would not have been done as smoothly.

And finally, I am thankful to all the subjects who participated and spent their time to help me in collecting measurements and validating our concept.

TABLE OF CONTENT

Page

LIST OF TABLES

Table Page

LIST OF FIGURES

Chapter 1
INTRODUCTION

Doppler Radar is a very versatile instrument to measure movements and velocity of vehicles, storms and celestial objects. In 1975 it was shown that a Microwave Doppler radar can also be used to remotely sense pulmonary motion[1]. This gave way to a range of research and applications for heart and respiration rate detection and estimation such as, remote monitoring of infants or adults to detect apnea[2] , detection of life through walls for defense and security operations[3], search rescue of survivors under earthquake rubble[4]. Since microwave can also penetrate walls and debris, this making Doppler radar an apt tool for search and rescue operation. The technology has also been demonstrated in rescue of an infant under rubble in Japan during an earthquake in October 2004[1]. Contact-less monitoring of vital sign is also a requirement for skin burn patients and infants at risk of Sudden Infant Death Syndrome (SIDS), where radar based detection would be a viable solution.

1.1 Radar Overview

RAdio Detection And Ranging (RADAR) is an device which uses radio waves to determine range, altitude or velocity of objects. Radar was developed during World War II by many nations for air-defense and ocean surveillance. Since then radar have been used in many diverse fields including, radio astronomy, antimissile systems, aircraft anti-collision systems, air traffic control, weather studies and ground penetrating radar for geological studies.

Radar consists of a transmitter which emits radio signal through an antenna in a particular direction of interest as portrayed in Figure 1. This emitted radio wave propagates through air and when these waves strike an object they reflect and scatter off the object's surface. The strength of the reflection depends on the dimensions and dielectric properties of the

[1] Reported by Nipponia on 15th June 2005 in issue No. 33:
http://web-japan.org/nipponia/nipponia33/en/feature/feature03.html

object. The small portion of this reflection propagates back in the direction of the radar which is sensed by the receiver of the radar. Since the radio waves reflect off from most large objects in the environment such as ground, trees, buildings, water etc., the reflection from the target, which is the signal of interest, is hard to detect amongst the unwanted clutter signal from rest of the environment. The backscattered signal is usually weak and it is amplified and sophisticated signal processing is done to separate the signal of interest from clutter.

The range of the target object is determined by measuring the delay between transmission and reception of the radar signal. The direction of the object is estimated from the direction of arrival of the signal. The relative velocity of the object is estimated by measuring the rate of change of distance or through the frequency shift in the reflected signal due to the Doppler Effect.

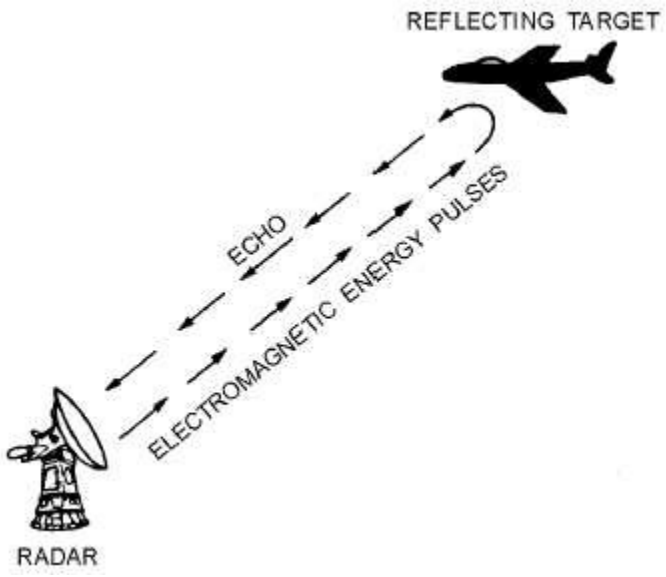

Figure 1: Principle of Radar

Radar can be broadly classified as:

1. Pulse radar
2. Continuous wave (CW) radar

Pulse radar transmits a train of short pulses of radio signal and measure the time of arrival (TOA) of these pulses to estimate the distance of the target. The velocity of the target can be estimated through the rate of change of measured distance. Continuous Wave radar transmits a continuous signal unlike a pulse radar and the major CW radars are 1) Doppler radar and 2) Chirp radar or Frequency modulated Continuous wave (FM-CW) radar.

Doppler radar is used when precise velocity of the target is to be estimated. It is based on the Doppler Effect, i.e. the reflected signal undergoes a frequency shift which is directly proportional to the relative velocity of the target with respect to the receiver. The Doppler frequency shift is expressed as follows,

$$\Delta f = \frac{\Delta v}{c} f_o \tag{1}$$

where Δf is the frequency shit observed, Δv is th relative velocity between the target and the receiver, f_o is the frequency of the emitted wave and c is the speed of EM wave.

Chirp radar is has the best of both pulse radar and Doppler radar as it can measure both velocity and range of the target. Chirp radar transmits a signal which has a varying frequency over time also called a sweep or chirp signal. By measuring the delay of the received signal the range is estimated and by measuring the frequency shift the velocity is estimated.

1.2 Radar for Vital Sign Estimation

As discussed earlier Doppler radar is an ideal instrument to measure subtle motion and for vital sign estimation ranging of the subject is not of prime interest. Hence, the vital signs are detected by transmitting an EM wave using a Doppler radar towards the subject under observation and the backscatters are sensed by the receiving antenna as illustrated in Figure 2. The reflections off the person's chest are phase modulated by the oscillations of the chest wall due to respiration and heart beat. It has been observed that the chest wall of a human is displaced between 4 – 12mm by respiration and about 0.6mm by heart beat

[5]. These minute motions induce a Doppler phase shift on the transmitted signal and the goal is to measure this to estimate the respiration and heart rate. The phase shift $\theta_b(t)$ is expressed as,

$$\theta_b(t) = \frac{4\pi x(t)}{\lambda} \tag{2}$$

Here $x(t)$ is the oscillatory motion of the chest wall and λ is the wavelength of the transmitted signal as portrayed in Figure 2. The Phase offset $\theta_b(t)$ is derived as the product of round trip time, $2x(t)/c$ and angular frequency, $2\pi f_o$ at the receiver resulting in $\frac{4\pi f_o x(t)}{c} = \frac{4\pi x(t)}{\lambda}$.

Since Doppler radar is sensitive to motion, any body motion will produce a phase shift on the received and adversely corrupt the intended signal of heart and respiration. Moreover, since body motion generally is random in nature (not oscillatory like respiration or heat beat) filtering its Doppler phase shift from the received signal is challenging. Also, if multiple subjects are standing in the view field of the antenna it is hard to isolate the vital sign of anyone of the subject.

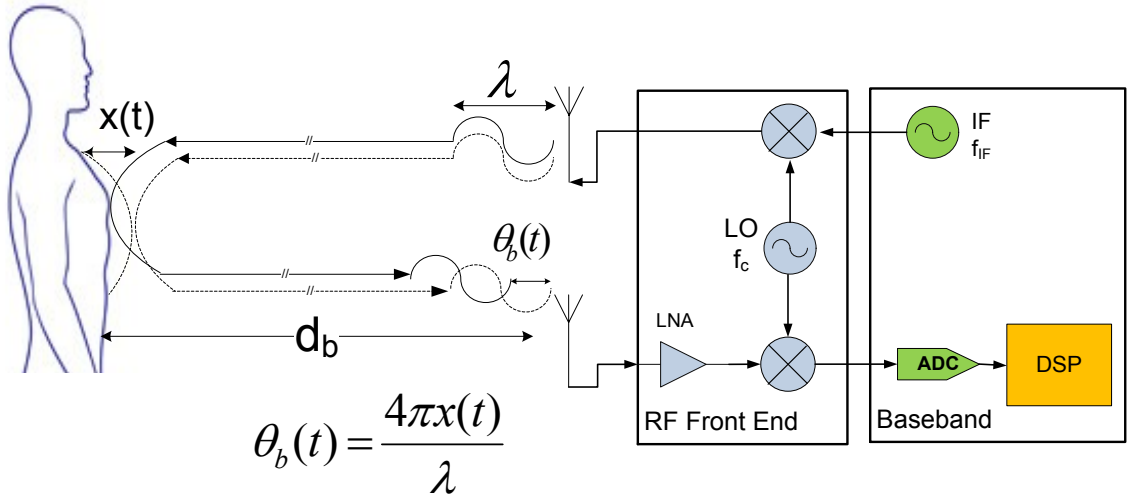

Figure 2: Principle of Doppler radar for vital sign estimation

1.3 Challenges for Vital Sign Detection

Over the years many problems have been identified which are inherent to Doppler radar and problems that are specific to vital sign detection. The problems that are inherent to Doppler radar are:

1. Phase noise
2. Clutter
3. Null-Point

The challenges that are specific to vital sign detection are:

1. Extremely close spaced Doppler shift to the carrier within range of 0.1-2 Hz.
2. Interference of respiration harmonics with heart signal [6].
3. 1/f noise
4. Random body motion
5. Vital sign estimation of multiple subjects

Many architecture and signal processing based solution have been suggested and are discussed in the following section.

1.4 Prior work

A lot has been accomplished in this field since the 1970s due to the advent of low cost integrated circuits, such as the design of Miniaturized IC based solutions in [2] and [7]; multiple RF architectures including homodyne, low-IF, and injection loop in [8], [9] and [10]; and the detection of multiple subjects through MIMO in [11] and [12]. Recently, it has been shown that the random body motion can be cancelled using multiple transceivers placed in front and behind a subject in [13] and [14]. For body motion cancellation differential font-end Doppler radar has also been demonstrated in [15]. Here dual helical antennas with a narrow beamwidth of 40^{o} illuminate adjacent locations on the subject's torso such that only one beam illuminates the heart and the signal from the second beam is used for body motion cancellation. The progress has been broadly made

in RF front end architecture and Baseband signal processing to estimate vital signs, few of these are listed in the following sections.

1.4.1 RF Front End Architecture

RF front end plays a pivotal role in minimizing the system noise, rejecting background clutter and mitigating other interferences. Apart from the classic homodyne and heterodyne architectures, direct IF sampling and self-injection locking architectures have recently been reported [8], [9], [10]. In the following section we discuss the fundamental homodyne and heterodyne architectures.

1. Homodyne

   Homodyne architecture transmits a power boosted LO signal at a specific frequency and at the receiver the received signal is down-converted to DC using the same LO. Though, this architecture is simple but it suffers with Null Point problem, 1/f noise and DC offset due to LO mixer coupling. To resolve the Null point problem a simple solution is to use a quadrature demodulator [16] as shown in Figure 3. DC offset can be avoided by having an intermediate frequency as in a heterodyne architecture.

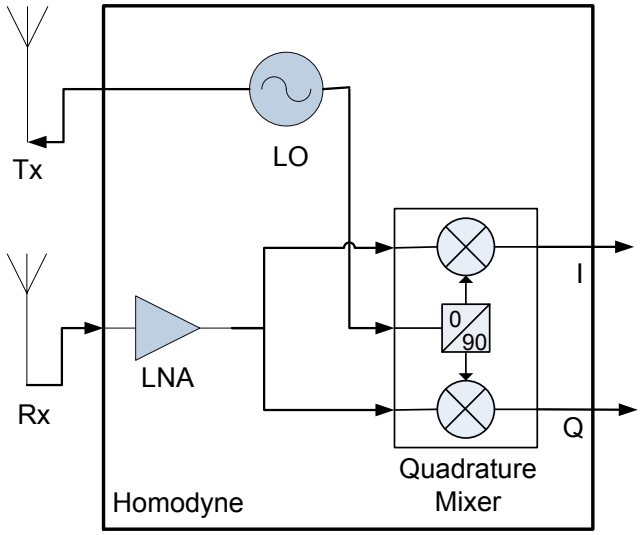

Figure 3: Simplified homodyne Doppler radar with quadrature receiver

2. Heterodyne

   In a heterodyne architecture for transmission an IF signal is up-converted by mixing it with an LO signal and the received signal is down-converted to DC by mixing it with

LO followed by the IF signal as show in Figure 4. To resolve the null point problem quadrature demodulation, phase tuning [17] or antenna and frequency diversity [18] can be used. Heterodyne receive are robust to DC offset, though it still suffers with 1/f noise.

As explained both homodyne and heterodyne architectures have their advantages and disadvantages. To overcome the 1/f noise and DC offset in this work a heterodyne receiver with direct IF sampling is implemented to estimate vital sign. This approach avoids the 1/f noise, DC offset and also avoids I/Q imbalance as the digital IF signal used for down-conversion in digital domain is perfectly orthogonal unlike the analog IF signal. The direct-IF signal is further discussed in detail in Chapter 2.

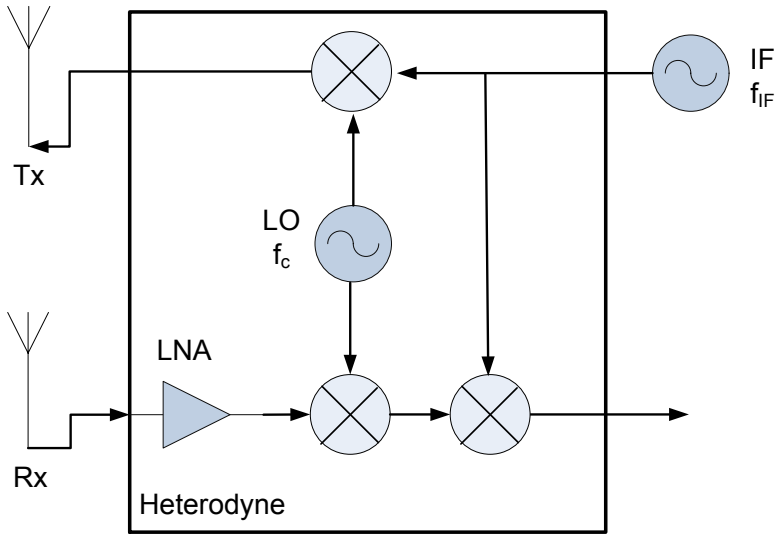

Figure 4: Simplified heterodyne Doppler radar.

1.4.2 Baseband Signal Processing methods

Once the received signal is down-converted to baseband using a suitable architecture digital signal processing techniques are used to estimate heart beat and respiration rate. The received baseband signal carries information of vital sign along with multiple noises, clutter, undesired body motion and possible vital signs of other unintended subjects, thus making desired vital sign estimation a challenging task.

For estimation of respiration and heart rate, arc-tan demodulation followed by Fourier transform (STFT) or autocorrelation to obtain the power spectrum has been suggested in

[2], [19] and [20]. This method separates the heart signal from respiration signal by a high pass filter with a cut-off of 0.7Hz (42bmp). It is observed that the harmonics of the respiration can exist beyond 0.7Hz [6]. Moreover, the second harmonic has comparable power to heart signal defeating the purpose of the high pass filter. Also, arc-tan demodulation requires DC offset calibration and is sensitive to any additive component like strong presence of clutter [19]. Hence a successful robust algorithm should be able to segregate the respiration harmonics and heart signal without a band limited assumption in presence of clutter and for such scenario super-resolution spectrum estimations, like MUltiple SIgnal Classification (MUSIC) algorithm, could resolve the problem. MUSIC was used for through wall detection of life and was able to detect respiration of a person behind a wall [3].

1.5 Proposed Approach

In this literature we concentrate on fundamental issues of transceiver architecture design and estimation of vital sign of a single resting subject, keeping body motion cancellation and multiple subject detection for a future discourse.

As pointed earlier, homodyne and heterodyne architectures have limitation and to circumvent these we have adopted a heterodyne architecture with direct IF sampling. We mitigate 1/f noise, I/Q imbalance and DC offset problems by directly digitizing the received IF signal and down-converting it to DC in digital domain, this method was also recently adopted in [21]. We also propose Adaptive Clutter Cancellation for a Low-IF architecture and Pattern Search in Noise Subspace (PSNS) algorithm to detect Doppler shift due to respiration and heartbeat. PSNS is an enhancement to MUSIC algorithm which using the knowledge of transmitted phase noise to enhance Doppler shift detection making it immune to spurious peaks due to phase noise. Using these techniques estimation of heart and respiration rate up to 6m has been achieved.

Experiments have been conducted over a small group of eight males and females over different distances to study the performance of the proposed system and algorithms. The primary interest of this work is to treat the known problems in a different light and

propose novel signal processing algorithms not been discussed earlier. A comprehensive study of the performance over large diverse population in terms of age, build and gender remains a study of further work.

1.6 Thesis Outline

The following literature starts with the description of the transceiver architecture with the corresponding signal analysis followed by the consideration made for architecture design in Chapter 2. In Chapter 3 the signal processing algorithms employed to extract heart and respiration signal have been discussed. In Chapter 4 the hardware adopted to realize a prototype system is discussed with their respective specification and measurements. Also, the simulation model developed to help study different architectures and algorithms virtually have been described here. The experiments carried out with their measurements and observations are also shared in Chapter 4. Finally, in Chapter 5 conclusion are drawn and the outline for future work has been suggested.

Chapter 2

TRANSCEIVER ARCHITECTURE

The RF front end plays a pivotal role in enhancing the sensitivity and range of vital sign measurement by minimizing the system noise, rejecting background clutter and mitigating other interferences. To avoid 1/f noise, DC offset due to LO leakage and I/Q imbalance a heterodyne architecture with direct IF sampling has been implemented as shown in Figure 5.

In following section, the requirements of the transmitter are discussed, followed by the design employed and the mathematical representation of the transmitted signal. The reflection of the signal from the person under observation and the environment is explained and mathematically formulated in Section 2.2. Finally, the receiver requirements, design adopted to mitigate each noise source, the baseband equivalent and mathematical representation of each received signal component is detailed in Section 2.3.

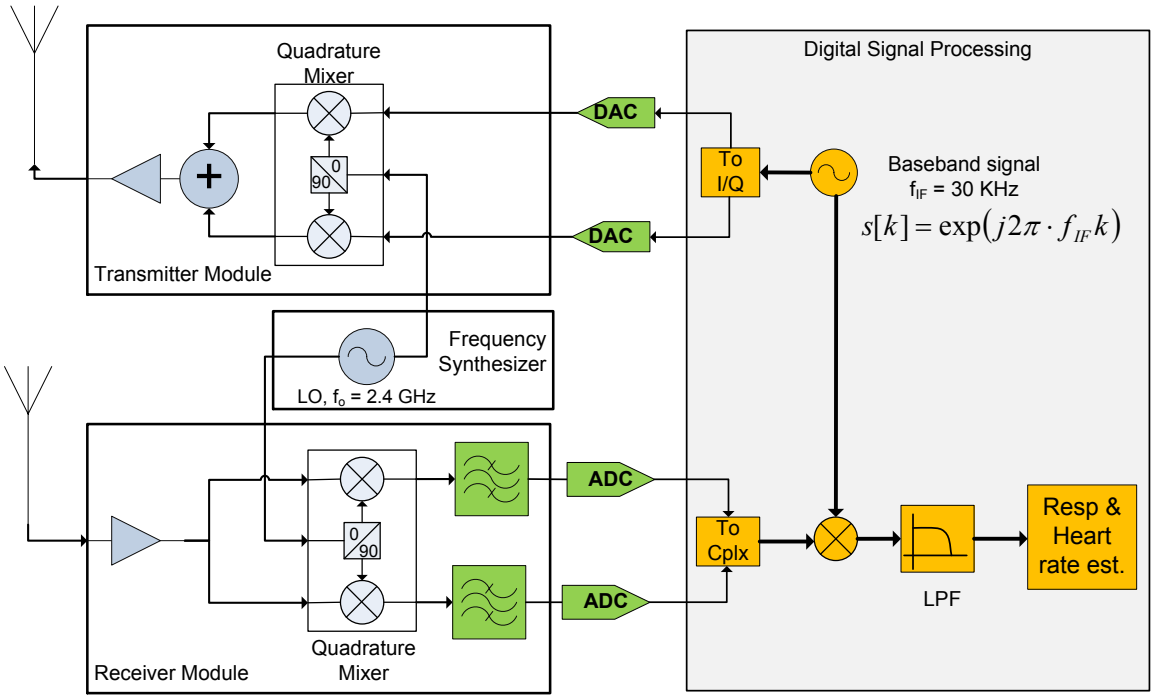

Figure 5: Transceiver Architecture with IF sampling

2.1 Transmitter

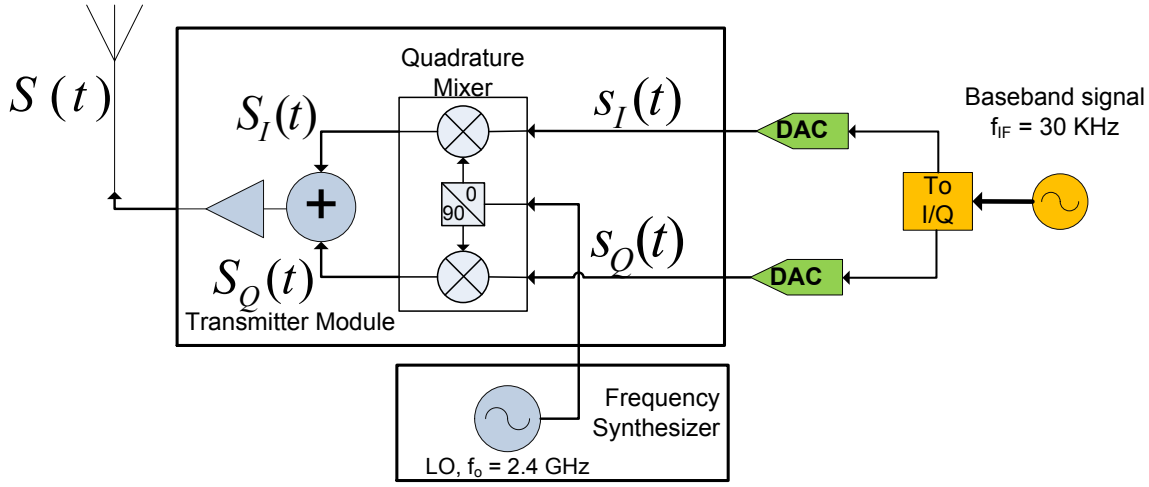

Figure 6: Low-IF quadrature transmitter

2.1.1 Requirement

The transmitter of a Doppler radar transmits a continuous single tone at a suitable frequency and power. Following are the major considerations for transmitter design:

1. **Radio Frequency**: For vital sign detection and estimation the transmit signal wavelength should be comparable to the displacement of the chest wall (in order of millimeters) to be detected. Also the choice of frequency impacts the ability of the radar signal to penetrate obstacles such as clothing, walls and debris blocking the subject. Higher frequency signal are more sensitive to smaller motion whereas lower frequency signal have higher penetration through obstacles. Hence the choice of frequency is a tradeoff between sensitivity to motion and permeability of the signal. S-band (2 – 4GHz) signal with wavelength 75mm – 150mm is adequately sensitive to estimate respiration and heart rate and can sufficiently penetrate obstacles, especially the lower S-band frequencies. Moreover, S-band RF circuits are widely used and inexpensive to develop.
2. **Tx-Rx isolation**: The transmit power impacts the operating range of the Doppler radar and is limited by the isolation between the Tx-Rx path, as Tx-Rx coupling

could saturate the receiver amplifiers making it insensitive to signal of interest. In a monostatic configuration, that is a single antenna for transmission and reception with a circulator to separate the transmission and reception path, the Tx-Rx isolation is equivalent to the isolation of the circulator used which at best provides 20dB isolation at 2.4GHz. For a bistatic configuration, which has two separate antennas for transmission and reception, 50dB isolation can be achieved when directional antennas are used.

2.1.2 Design

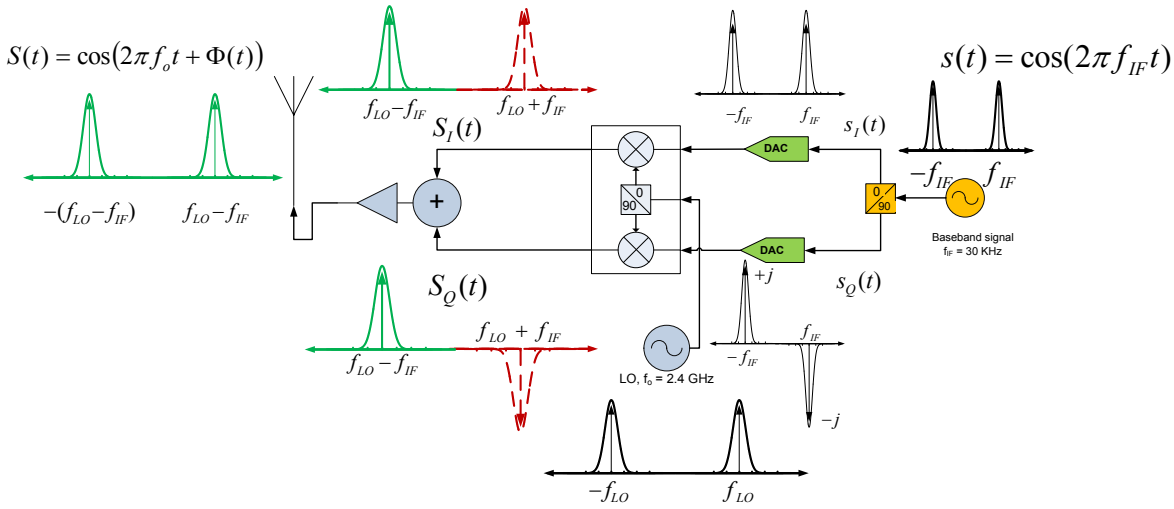

Figure 7: Single Side Band Transmission.

The transmitter, as illustrated in Figure 6, has an LO which generates the RF signal and is mixed with the baseband IF signal through a Quadrature mixer to obtain a single side band transmission signal, $S(t)$. The Quadrature IF signal $s(t)$ is at a nominal frequency of few KHz generated digitally or by using an analog oscillator as show in Figure 6. The low-IF architecture is adopted to avoid 1/f noise and DC offset due to LO leakage at the receiver [8].

The baseband quadrature signal $s(t)$ is generated with amplitude A at intermediate frequency f_{IF} and is expressed as,

$$s(t) = A \cdot e^{j(2\pi f_{IF} t)} \tag{3}$$

Here we ignore the phase noise generated at the baseband, as it is smaller than the LO's phase noise.

$$\begin{aligned} s_Q(t) &= Im\left(e^{j(2\pi f_{IF} t)}\right) = A \cdot \sin(2\pi f_{IF} t) \\ s_I(t) &= R\left(e^{j(2\pi f_{IF} t)}\right) = A \cdot \cos(2\pi f_{IF} t) \end{aligned} \tag{4}$$

The analog quadrature components of the baseband signal $s_Q(t)$ and $s_I(t)$, as expressed in (4) are mixed with LO signal at f_{LO} frequency to obtain up-converted $S_Q(t)$ and $S_I(t)$ as illustrated in Figure 7 (the RF signal is represented in uppercase letters and baseband signal is expressed in lowercase letters) and are expressed as,

$$\begin{aligned} S_Q(t) &= A \cdot \sin(2\pi f_{IF} t) \cdot \sin\left(2\pi f_{LO} t + \Phi(t)\right) \\ &= \frac{A}{2} \cdot \{\cos\left(2\pi (f_{LO} - f_{IF})t + \Phi(t)\right) \\ &\qquad - \cos\left(2\pi (f_{LO} + f_{IF})t + \Phi(t)\right)\} \end{aligned} \tag{5}$$

$$\begin{aligned} S_I(t) &= A \cdot \cos(2\pi f_{IF} t) \cdot \cos\left(2\pi f_{LO} t + \Phi(t)\right) \\ &= \frac{A}{2} \cdot \{\cos\left(2\pi (f_{LO} - f_{IF})t + \Phi(t)\right) \\ &\qquad + \cos\left(2\pi (f_{LO} + f_{IF})t + \Phi(t)\right)\} \end{aligned} \tag{6}$$

Here $\Phi(t)$ is the phase noise generated by the LO. The up-converted quadrature components are added to eliminate the upper-side band and transmit the lower-side band as shown in (7).

$$\begin{aligned} S(t) &= S_Q(t) + S_I(t) \\ &= A \cdot \cos\left(2\pi (f_{LO} - f_{IF})t + \Phi(t)\right) \end{aligned} \tag{7}$$

The transmitted signal can also be concisely expressed in complex form as,

$$\begin{aligned} S(t) &= R\left\{A \cdot e^{j\left(2\pi\,(f_{LO} - f_{IF})t + \Phi(t)\right)}\right\} \\ &= A\cos\,(2\pi\,(f_{LO} - f_{IF})t + \Phi(t)) \end{aligned} \tag{8}$$

Hereafter for brevity $f_{LO} - f_{IF}$ will be expressed as f_o.

Due to the phase noise $\Phi(t)$ the LO signal is not a pure sinusoidal tone or an ideal delta function in frequency domain, rather the LO signal has a frequency skirt as illustrated in Figure 8. Due to imperfection in quadrature mixing the upper-side band and the carrier are not completely suppressed and some of it leaks to the transmitted signal, other than the desired lower-side band. The resultant spectrum of the transmitted signal $S(t)$ is as shown in Figure 9.

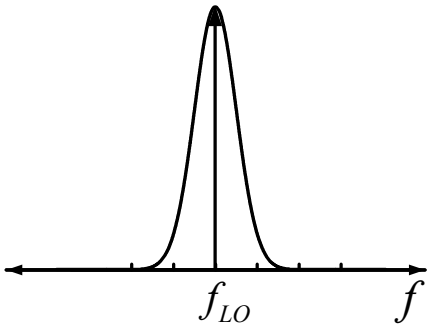

Figure 8: LO Spectrum (not to scale)

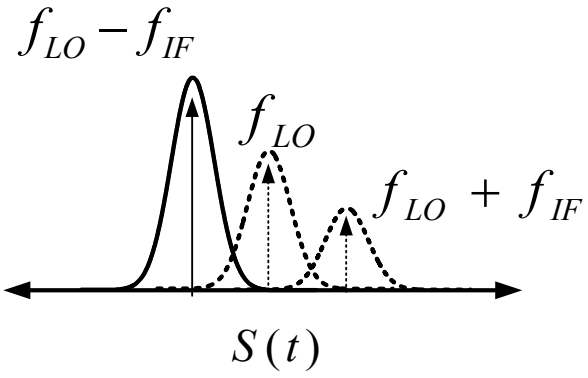

Figure 9: Transmitted signal spectrum (not to scale)

The phase noise at frequencies closer to the carrier is much larger than white noise. This drastically reduces SNR of the signal of interest at the receiver. Since phase noise is inherent to oscillators, little can be done at the transmitter to reduce phase noise

especially when a stringent requirement of low phase noise within one hertz of the carrier is required. Phase noise is reduced to an extent at the receiver through phase noise filtering using range correlation effect, which is achieved by having coherent receiver and transmitter. But, even after phase noise filtering the residual still makes the Doppler shift detection challenging and this is overcome through the PSNS algorithm proposed in this work. Phase noise filtering is further explained in the following sections.

2.2 Reflected Signal

The signal $S(t)$, transmitted through the transmit antenna towards the person under observation is reflected from the person's body and the surrounding environment. As shown in Figure 10, a small portion of the reflection from the person body as wells as from the environment is backscattered towards the receiving antenna. Also, a portion of transmitted signal itself leaks to the receiver antenna depending on the isolation between transmit and receive paths.

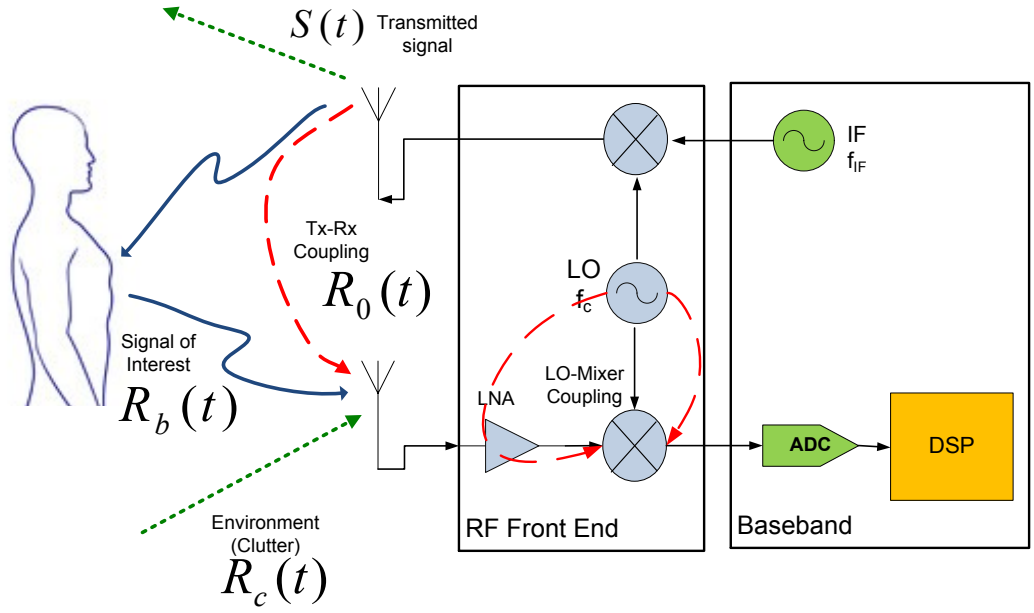

Figure 10: Received signal components

Hence the received signal $R(t)$, is a sum total of:

1) signal of interest $R_b(t)$, the backscatter from the subject's torso

2) the clutter $R_c(t)$, the backscatter from the stationary environment in the view field of the antenna including the rest of the subject's body
3) the transmitter-receiver leakage $R_0(t)$

The received signal is expressed as,

$$R(t) = R_b(t) + R_c(t) + R_0(t) + Z(t) \tag{9}$$

here $Z(t)$ is Additive White Gaussian Noise (AWGN).

2.2.1 Clutter

The clutter signal is a sum of delayed and attenuated versions of the transmitted signal as everything other than the subject's torso is assumed to be stationary and hence can be analytically represented by,

$$R_c(t) = \sum_{i=0}^{N} \alpha_i \cdot \cos\left(2\pi f_o t + \frac{4\pi d_i}{\lambda} + \Phi\left(t - \frac{2d_i}{c}\right)\right) \tag{10}$$

Here, c is the speed of EM wave, λ is its wavelength, N represents arbitrary number of reflection paths, α_i and d_i are their respective amplitudes and distances. We also include the leakage component $R_0(t)$ as the zeroth paths of clutter, since it too is delayed and attenuated version of the transmitted signal.

The clutter is the strongest component of the received signal, due to the large radar cross-section area of the environment compared to a human heart and chest. Even though the clutter, respiration and heart are separated by frequency, but due to phase noise clutter significantly corrupts the signal of interest as illustrated in Figure 11. The phase noise skirt of clutter increases the noise floor in the neighboring frequencies, thereby reducing the SNR of signal of interest.

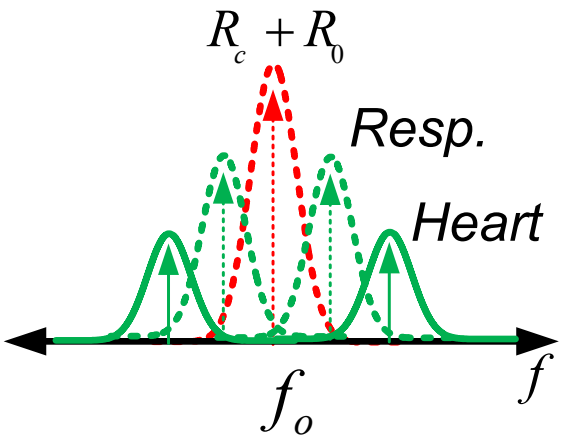

Figure 11: Received signal power spectrum

2.2.2 Signal of interest

The signal reflected from the stationary person's chest-wall is phase modulated by its movement $x(t)$ due to respiration and heart beat [5], [22] and can be expressed as

$$R_b(t) = \alpha_b \cdot \cos\left(2\pi\, f_o t - \frac{4\pi d_b}{\lambda} - \frac{4\pi x(t)}{\lambda} + \Phi\left(t - \frac{2d_b}{c}\right)\right) \tag{11}$$

Here, d_b is the distance of the person from the radar. A simple model of the oscillatory motion of the chest wall can expressed as $x(t) = \mathrm{A_r}\cos(2\pi f_r t) + \mathrm{A_h}\cos(2\pi f_h t)$ [2], [22].

The signal of interest is weak compared to clutter due to the small RCS of human heart and chest. The phase noise skirt of clutter further reduces the SNR. Moreover, the Phase noise of respiration and its harmonics also reduce the SNR of the heart signal as portrayed in Figure 11, making detection of heart rate over large distance challenging.

2.3 Receiver

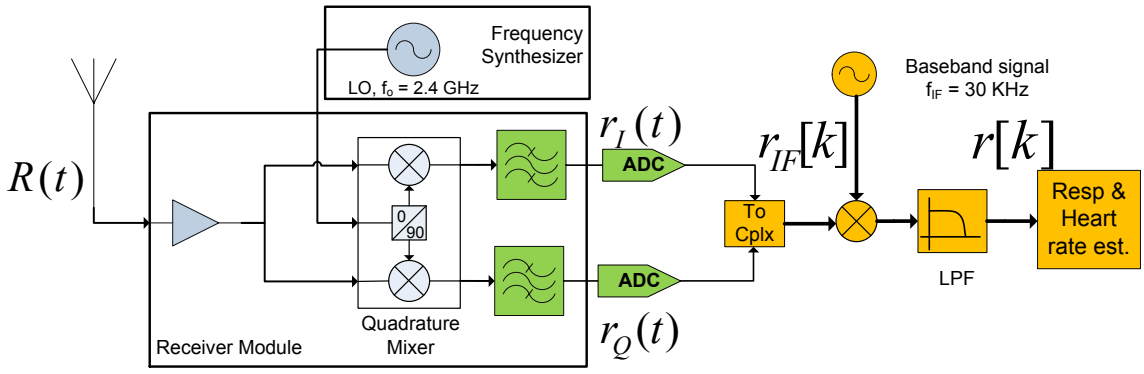

Figure 12: Quadrature receiver

2.3.1 Requirement

The requirements of the receiver module are:

1. Maximize SNR
2. Avoid null point
3. Suppress image frequency

The reflected signal expressed in (9) is sensed by the receiving antenna and is down converted to baseband by the receiver to estimate the Doppler shift. To estimate the vital sign from the received signal an adequate SNR is required. There are multiple noise sources at the receiver which include Phase noise, AWGN, clutter, $\frac{1}{f}$ noise and DC offset due to mixer-LO coupling. Flicker noise and DC offset originate at the receiver unlike the rest of the noise sources which originate at the transmitter or from the channel. The SNR of the received signal can be expressed as,

$$SNR = \frac{\sigma\,\overline{x^2(t)}}{N_z + N_{\frac{1}{f}} + N_{\Delta\Phi}} \tag{12}$$

Where, σ is the RCS of chest and heart, N_z is the AWGN power, $N_{\frac{1}{f}}$ is the 1/f noise power and $N_{\Delta\Phi}$ is the phase noise power contributed by the phase noise skirt of clutter at baseband. The Phase noise is reduced by having a coherent demodulation at the receiver, utilizing the range correlation effect. The residual phase noise power $N_{\Delta\Phi}(f)$ is expressed as,

$$N_{\Delta\Phi}(f) \approx 2N_{\Phi}(f)\left(16\pi\left(\frac{d}{c^2}\right)\right) \tag{13}$$

The phase noise floor is proportional to the delay of the received signal [23] and leads to reduction in SNR for large distances as implied by (13). The SNR of the cardiopulmonary signal is expressed in detail by Droitcour *et al*. in [24].

Unlike other sources of noise, $\frac{1}{f}$ noise can be completely avoid by using a Low–IF architecture [8]. Thus we have adopted a Low-IF architecture with f_{IF} chosen such that the 1/f noise is less than the thermal noise at that frequency as shown in Figure 13. Moreover, low-IF also aids in avoiding the DC offset due to LO leakage.

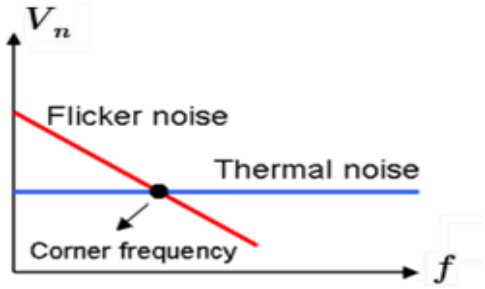

Figure 13: 1/f noise corner frequency

The received signal is sensitive to the distance of the person d_b under observation as implied by (11). The received signal when down-converted to DC tends to zero when $\frac{4\pi d_b}{\lambda}$ is an odd integer multiple of $\pi/2$, such points are called Null Points. Multiple solutions to circumvent Null Point problem have been suggested including: 1) phase tuning in [17], where the transmitted signal is imparted phase offset so as to effectively

shift the null point in space, 2) antenna and frequency diversity in [18], by which the effect wavelength λ or distance d_b is varied and 3) Quadrature demodulation which is discussed in detail in the following section. Quadrature demodulation is effective and simple in terms of hardware implementation and hence it has been adopted.

2.3.2 Design

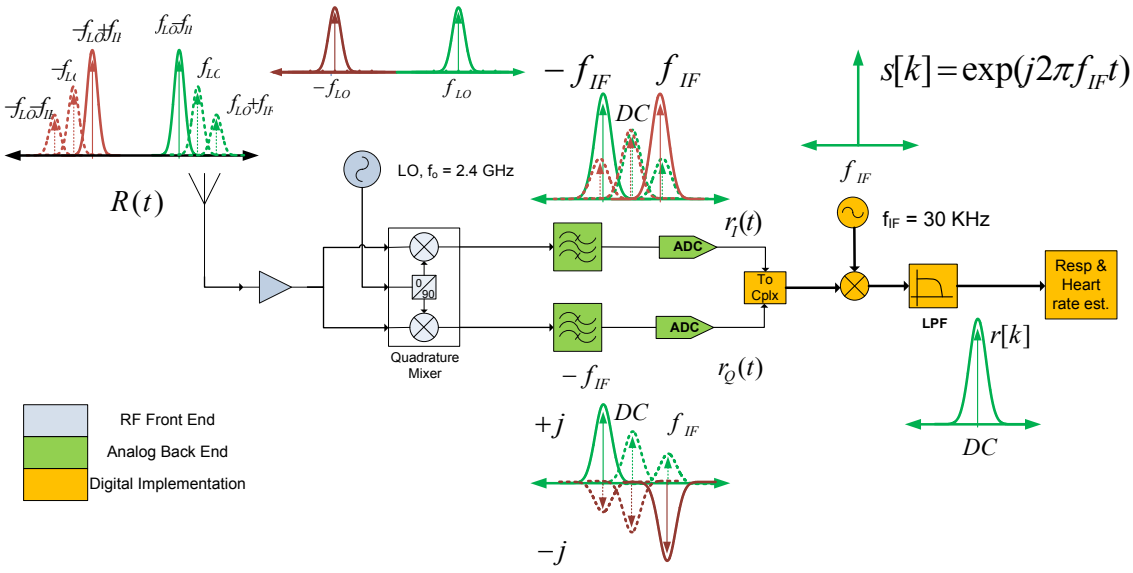

Figure 14: Receiver with image suppression

Figure 14 illustrates Weaver architecture with direct IF sampling to suppress image frequency and avoid 1/f noise. To extract respiration and heart rate we need to analyze $x(t)$, hence the received signal is coherently down-converted by mixing it with the same LO signal through a quadrature mixer. The I/Q components after mixing it with the LO signal are expressed as,

$$r_I(t) = R(t) \cdot \cos\left(2\pi f_{LO} t + \Phi(t)\right) \quad (14)$$

$$r_Q(t) = R(t) \cdot \sin\left(2\pi f_{LO} t + \Phi(t)\right) \quad (15)$$

Down-converted signal of interest (R_b), $r_b(t)$ is deducted as follows, the in-phase component

$$r_{b,I}(t) = R_b(t) \cdot cos\big(2\pi f_{LO} t + \Phi(t)\big) \tag{16}$$
$$= \frac{\alpha_b}{2}\{cos(A-B) + cos(A+B)\}$$

$$r_{b,Q}(t) = R_b(t) \cdot sin\big(2\pi f_{LO} t + \Phi(t)\big) \tag{17}$$
$$= -\frac{\alpha_b}{2}\{sin(A-B) - sin(A+B)\}$$

Here, $A = 2\pi(f_{LO} + f_{IF})t + \Phi\left(t - \frac{2d_b}{c}\right)$ and $B = 2\pi(f_{LO})t + \Phi(t)$. Simplifying (16) and (17) further and ignoring the higher frequency component $(A+B)$ as it will be filtered out, we get,

$$r_{b,Q}(t) = -\frac{\alpha_b}{2} \cdot \sin\left(2\pi f_{IF} t + \frac{4\pi d_b}{\lambda} - \frac{4\pi x(t)}{\lambda} + \Delta\Phi(t)\right) \tag{18}$$

$$r_{b,I}(t) = \frac{\alpha_b}{2} \cdot \cos\left(2\pi f_{IF} t + \frac{4\pi d_b}{\lambda} - \frac{4\pi x(t)}{\lambda} + \Delta\Phi(t)\right) \tag{19}$$

Where, $\Delta\Phi(t) = \Phi\left(t - \frac{2d_b}{c}\right) - \Phi(t)$ is the residual phase noise. As we can see from (19) and (20) that irrespective of the distance d_b, either in-phase or quadrature-phase component is non-zero at any give distance. Hence Quadrature receiver inherently resolves the Null point issue.

The down-converted IF signal of interest ($R_b(t)$) can also be concisely expressed in complex form as,

$$r_{IF,b}(t) = \alpha_b \exp\left(-j\left(\frac{4\pi d_b}{\lambda} - \frac{4\pi x(t)}{\lambda} + \Delta\Phi(t)\right)\right) \cdot s(t) \tag{20}$$

Here, $r_b(t) = \alpha_b \exp\left(-j\left(\frac{4\pi d_b}{\lambda} - \frac{4\pi x(t)}{\lambda} + \Delta\Phi(t)\right)\right)$ is the signal of interest at DC. Similarly, the down-converted clutter $r_c(t)$ component at DC can be deduced and expressed as,

$$r_c(t) = \sum_{i=1}^{N} \alpha_i \exp\left(j\left(\frac{4\pi d_i}{\lambda} + \Delta\Phi_i(t)\right)\right) \tag{21}$$

Here, residual phase noise of each path is, $\Delta\Phi_i(t) = \Phi\left(t - \frac{2d_i}{c}\right) - \Phi(t)$. Hence the down-converted received baseband signal can be expressed as the baseband equivalent of $R(t)$,

$$r_{IF}(t) = \{r_b(t) + r_c(t)\} \cdot s(t) + z(t) \tag{22}$$

$r_{IF}(t)$ consists of I/Q components and expressed in complex form using (20) and (21). The baseband signal is also low pass filtered and amplified before feeding to the ADC so as to utilize the complete dynamic range of the ADC and to eliminate the higher frequency components.

2.4 Clutter Cancellation

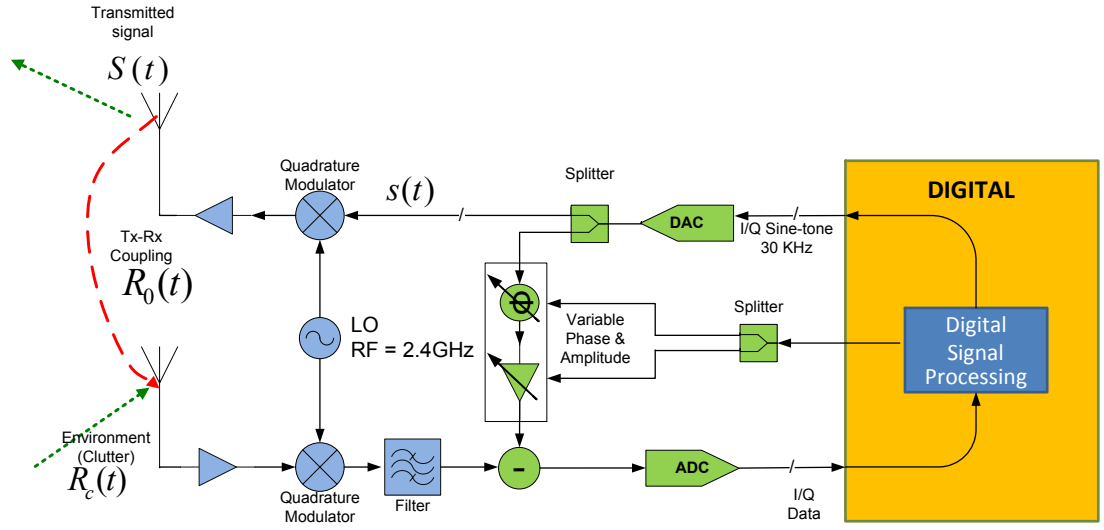

Figure 15: Baseband clutter cancellation

The clutter signal $r_c(t)$ is the strongest component of the received signal since the Radar Cross Section (RCS) of the background is much larger than the human torso, especially when detecting life behind walls or under rubble. Moreover, the transmitter-receiver leakage is substantial compared to the single of interest. Clutter can make the receiver insensitive to the weak signal from heart and respiration by saturating the receiver chain amplifiers and also dictate higher ADC resolution[4], [19], [25]. The leakage component also limits the transmit power and result in reduced range and sensitivity. As shown in Figure 15 and Figure 16 the clutter can be cancelled on the received path by subtracting attenuated and phase shifted transmitted signal in baseband or RF-front end. Clutter cancellation in Baseband is easier and can be accurately done due the low operating Intermediate frequency. While, clutter cancellation in RF front end can be challenging but this could allow monostatic configuration, reducing the form-factor of the system. The attenuation and phase of the received clutter signal is estimated digitally. A trial-and-error search method to estimate the attenuation and phase suggested in [4] works well and suit their requirement for one time estimate. But if the environment is not completely stationary or if the device is mobile as in [26], then it becomes mandatory to continuously estimate the clutter and cancel it. Digital estimation of attenuation and phase for adaptive clutter cancellation is further discussed in Section 3.1.1.

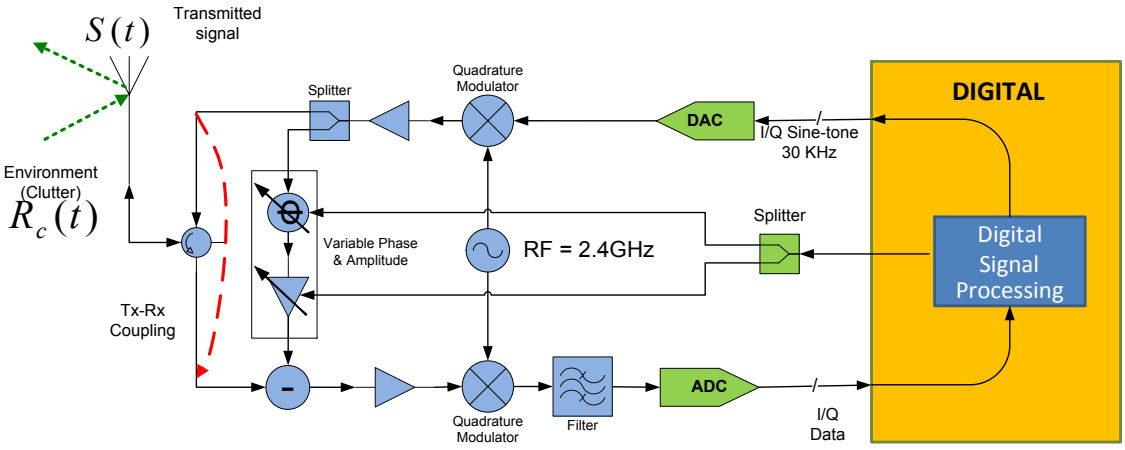

Figure 16: RF front-end clutter cancellation.

Chapter 3
SIGNAL PROCESSING

The goal of signal processing is to estimate the Respiration and Heart rate which are equivalent to the Doppler shift on the received signal. Doppler shift can be extracted by doing a spectral analysis of the received signal. Spectral analysis can be done through parametric or non-parametric methods. Non-parametric methods such as classic periodogram or the average periodogram (Welch's Method), make no assumptions of structure in the data to be analyzed. Parametric methods such as Autoregressive-moving-average model (ARMA), AR model or MA model, assumes an autoregressive or moving average process or both with a known order. Even though parametric methods could outperform non-parametric methods in certain applications they are not useful here since they are sensitive to the order of the model which is unknown.

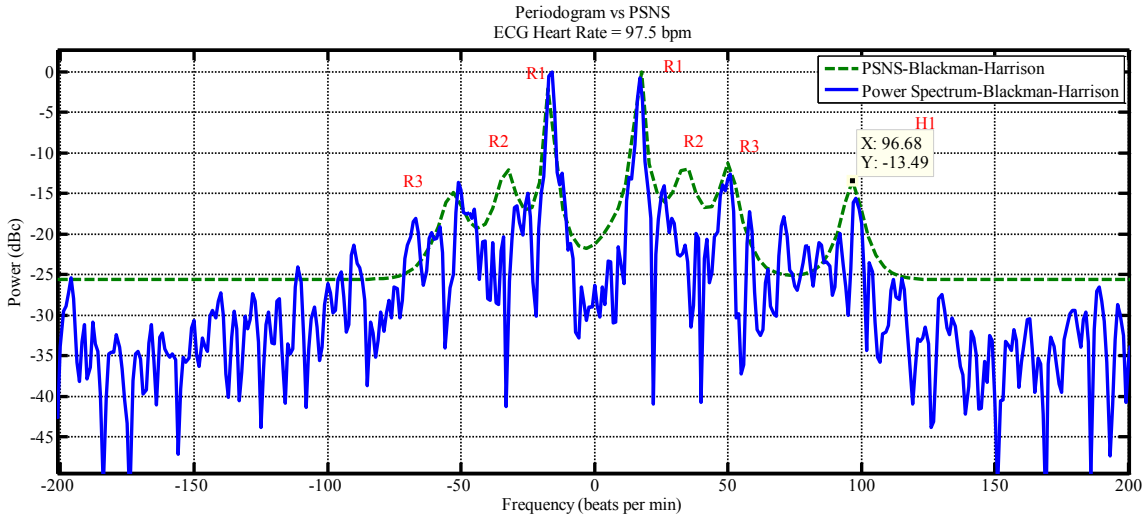

Figure 17: Typical Power Spectrum of a relaxed person seated at a distance of 6m.

$$P_{PER}(f) = \frac{1}{N}\left|\sum_{n=0}^{N-1} x[n]\exp(-j2\pi fn)\right|^2 \qquad (23)$$

Eq (23) is the periodogram spectral estimator of signal $x[n]$. As one can notice periodogram is computational efficient through Fast Fourier Transform (FFT) but its resolution is inversely proportional to observation interval, implying that to attain a resolution of 1 BPM a observation of 60 seconds is required. It has dominant side-lobes when the signal does not contain harmonically related sinusoids this can be alleviated to an extent through windowing but at a cost of frequency resolution. In Figure 17 solid line shows typical spectral content of an individual's measurement obtained using Priodogram with Blackman-Harrison window over 60 seconds interval. R1, R2 and R2 are respiration and its harmonics and H1being the heartbeat, the number of closely spaced frequencies making estimating respiration and heart beat difficult. Moreover, over 60 seconds the heart rate and respiration vary for a healthy individual rendering priodogram approach to an inherent error. To resolve the closely spaced respiration and heat signal high pass filtering with cut-off of 0.7Hz has been suggested followed by periodogram to obtain power spectrum. But it is observed that the harmonics of the respiration do exist beyond 0.7Hz [6].

Pitch detection technique from audio processing domain by using center clipping function to suppress spurious harmonics has been suggested by B. Lohman et al [20]. This method too segregates the heart and respiration signal through a high-pass filter followed by center clipping. Center clipper function clips the input below a known threshold Th, and expressed as,

$$r[k] = \begin{cases} r[k], & if\ |r(k)| > Th \\ 0, & else \end{cases} \qquad (24)$$

Clipping the input signal helps in enhancing the dominant harmonics and suppressing weaker ones. But since the power of the 2nd and 3rd respiration harmonics which are close to the heart signal are comparable, defining a threshold for centre clipping is difficult.

Hence a successful robust algorithm should be able to segregate the respiration harmonics and heart signal without a band limited assumption in presence of clutter and estimate vital signal over a short duration. For such scenario MUltiple SIgnal Classification

(MUSIC), a frequency estimations method, could resolve the problem. MUSIC algorithm was used for through wall detection of life and were able to detect respiration of a person behind a wall [3]. Here we propose a modified MUSIC algorithm which utilizes the information of the transmitted phase noise to enhance Doppler shift detection, which we have termed as Pattern Search in noise Sub-space (PSNS). In following section a comparison is drawn between Periodogram, MUSIC and PSNS methods.

3.1 Receiver Signal Chain

To accomplish estimation of respiration and heart rate the baseband analog signal is amplified and digitized through an ADC and can be represented as,

$$r_{IF}[k] = (r_b[k] + r_c[k]) \cdot s_{IF}[k] + z[k] \qquad (25)$$

Here, clutter signal $r_c[k]$ and signal of interest $r_b[k]$ are the digital equivalent of $r_c(t)$ and $r_b(t)$ respectively. $s_{IF}[k] = \exp(j2\pi f_{IF}k)$ is the digitized baseband transmission signal and $z[k]$ is the AWGN.

A number of operations are performed to make the digitized received signal $r_{IF}[k]$ ready for frequency estimation by using PSNS as illustrated in Figure 18. The received signal is first down-converted to DC digitally, which is done to avoid $\frac{1}{f}$ noise, and then it is filter and decimated to more tractable sampling frequency. Further, covariance matrix is estimated over windowed data and this covariance matrix is finally used by PSNS to estimate the heart and respiration rate. Also, the adaptive clutter cancellation done in the analog domain needs the estimate of amplitude and phase of clutter which is estimated from the digitized baseband signal. By using these techniques accurate estimates of heart and respiration rate haven achieved up to 6m while transmitting at nominal -6dBm power. Each of these block are explained in detail in the following sections.

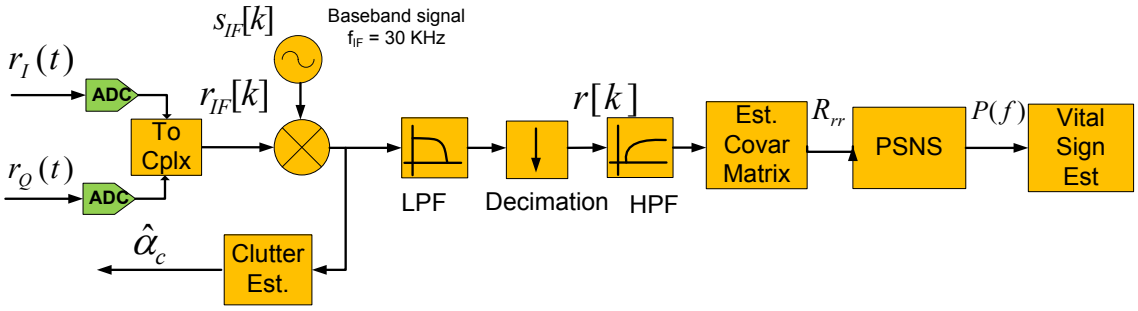

Figure 18: DSP receiver signal chain

3.1.1 Clutter Cancellation

The Clutter signal power depends on RCS of the reflector and their distance from the Radar, whereas, the leakage power depends on the isolation provided by the circulator in the mono-static case or Tx-Rx antenna isolation in bi-static case. Clutter is most severe for detection of life through wall or under earthquake rubble application. As show in (10) clutter is a summation of attenuated and phase delayed copies of the transmitted signal. Hence clutter can be cancelled by subtracting similarly attenuated and phase delayed transmission signal in analog domain as shown in Figure 19. This was demonstrated in [4] for detection of life under earthquake rubble. The phase and attenuation is estimated through the digitized signal, $r_{IF}[k]$ and the clutter component can be expressed as:

$$r_{IF,c}[k] \approx \left(\sum_{i=1}^{N} \alpha_i \cdot e^{(j\theta_i)}\right) \cdot s[k] + z[k] \qquad (26)$$

$$\approx \alpha_c \cdot e^{j\theta_c} \cdot s[k] + z[k]$$

Here, $r_c = \alpha_c \exp(j\theta_c)$ is the resultant of N clutter components including the leakage between transmit and receive path, $\theta_i = \frac{4\pi d_i}{\lambda}$ and $s[k] = \exp(j2\pi f_{IF} t + \Delta\Phi[k])$ is the baseband transmitted signal at f_{IF}. The phase noise of each path is assumed to be equal which is a valid approximation in an indoor environment.

Adaptive echo cancellation is a very well studied field in telephony and audio signal processing [27], [28], [29]. LMS was suggested in 1980s to adaptively estimate the impulse response of the echo path (hybrid circuit) [27]. A similar problem arises for a full duplex Relay and Ethernet networks [30]. The challenge here being, the received signal of interest and clutter signal are closely related and are only off by sub hertz, unlike the Telephony or the Relay scenario. A single tap LMS is sufficient due to constant phase delays of clutter components, as implied by (26).

Straight forward method to estimate the phase and amplitude at the IF frequency will be through a Fourier transform. To get the estimate of the clutter while filtering out the respiration and heart signal a Fourier transform over 10 seconds would have to be performed to attain a resolution of 0.1Hz. Here we present an LMS based Clutter cancelation which updates the phase and amplitude estimate every second. Its implementation is illustrated in Figure 19, where the darker blocks are implemented in analog and the lighter in digital.

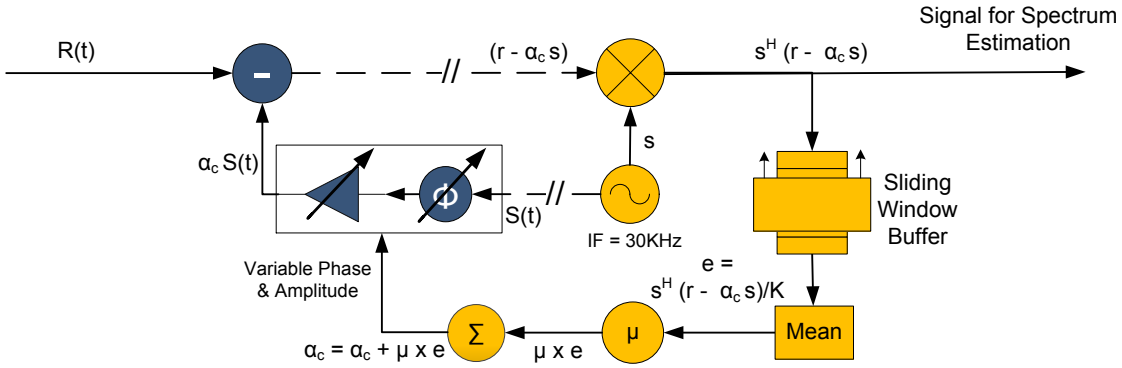

Figure 19: LMS filter based Clutter Cancellation.

An LMS filter if not setup with care can cancel the respiration and heart signal. The LMS equation is formulate as:

$$R(t) = R_{in}(t) - \hat{\alpha}_c \cdot S(t) \qquad (27)$$

Where $R_{in}(t)$ is the original signal received from the antenna as shown in Figure 19, $\hat{\alpha}_c$ is the estimate of the effective phase and amplitude of clutter in the received signal. $\hat{\alpha}_c$ is

estimated in baseband through the digitized baseband signal, $r_{IF}[k]$. In echo cancellation the know signal is subtracted from the received through an adaptive filter and the resultant error, here $R(t)$, is minimized. We instead match-filter the resultant error $R(t)$ with $S(t)$, or equivalently at baseband $r_{IF}[k]$ and $s[k]$ to obtain clutter amplitude and phase or LMS error i.e.

$$e = \frac{1}{K}\sum_{i=1}^{K} s[k]^H \cdot r_{IF}[k] \tag{28}$$

This match-filtered error e weighted by μ and is used iteratively to update the estimated phase and amplitude $\hat{\alpha}_c$,

$$\hat{\alpha}_c = \hat{\alpha}_c + \mu \cdot e \tag{29}$$

The match-filter in the LMS formulation and slow update over 1 second worth of samples (K) ensure the respiration and heart signal are not cancelled. Clutter cancellation effectively increases the sensitivity of the system by reducing the quantization noise and relaxes the requirement of a high resolution ADC. We have empirically observed that the heart signal is $\sim 25dB$ or $\sim 30dB$ below respiration signal for adult men and women respectively. Assuming a perfect Automatic Gain Control (AGC) ensuring the ADC is operated at full scale, 6-7 bit resolution should be sufficient for vital sign detection and can be deducted as follows,

$$\begin{aligned} SQNR &= 20\log_{10}(2^Q) + 10\log_{10}\left(\frac{3}{2}\right) \\ &= 6.02 \cdot Q + 1.76\ dB \end{aligned} \tag{30}$$

Taking $SQNR \geq 30dB \Rightarrow Q \geq 6\ bits$. Therefore, 12 bit ADC should be sufficient for vital sign detection application giving a liberal margin of $30dB$ below heart signal to avoid quantization noise and accommodate fluctuation. But, the respiration signal itself can be $30 - 50dB$ below clutter depending upon Tx-Rx isolation and the environment which increases the ADC requirement to $16 - 24$ bits. Hence by cancelling clutter and having an AGC we gain substantial reduction in ADC resolution requirement. In Figure

20 solid line represents the signal after clutter cancellation while dashed line represents the signal before clutter cancellation. One can clearly see that the clutter has been suppressed by 30dB and brought in power with respiration signal, clutter cancellation beyond this point is unnecessary as it would not reduce the number of ADC bits. 30dB reduction in clutter power directly corresponds to 5bit reduction in ADC requirement.

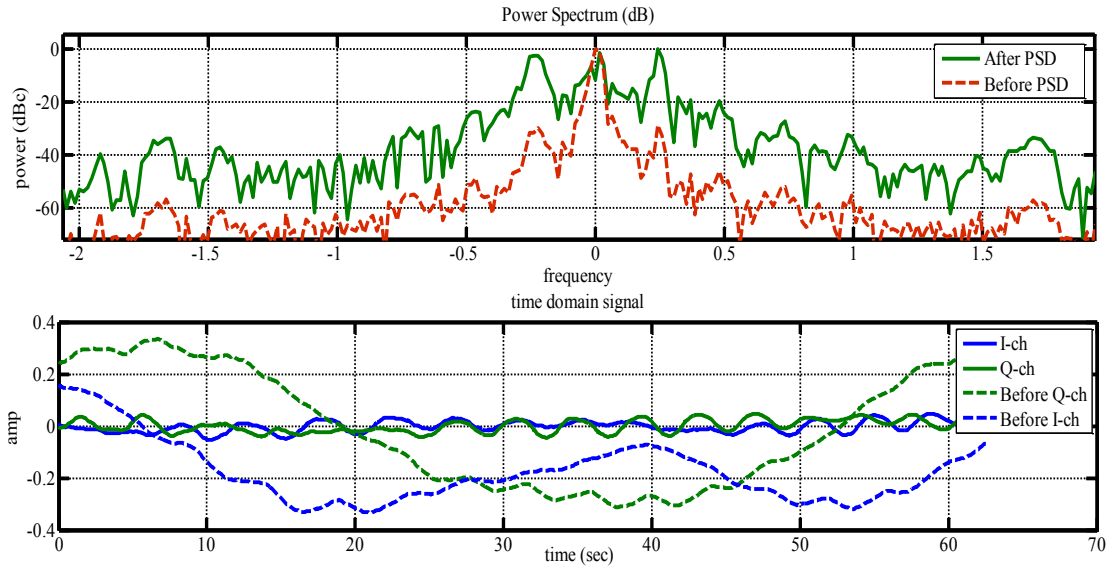

Figure 20: Clutter cancellation performance.

3.1.2 Filtering and Decimation

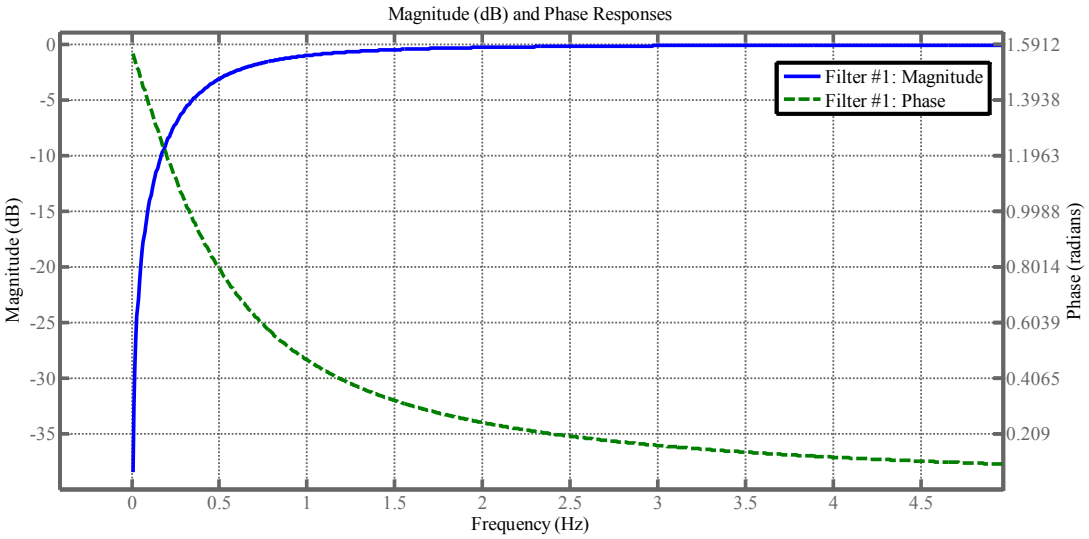

Figure 21: 1st order Butterworth high pass filter

Further in the receiver signal chain, as shown in Figure 18, the digital baseband signal is down-converted to DC, low pass filtered with an IIR filter having stop frequency of 5Hz and decimated to a sampling frequency of 10Hz. The signal at DC is further High pass filtered to block the residual clutter and attenuate the respiration and its harmonics with a 1st order Butterworth filter having a stop frequency of 0.05Hz and pass frequency of 1Hz as shown in Figure 21. This filter is important as it reduces the respiration signal's power and its corresponding phase skirt. This helps in reducing the signal subspace rank for subspace spectrum analysis (PSNS). IIR filter was chosen over FIR filter here even though it does not have a linear phase because no superior performance were observed with an FIR filter, moreover, FIR filter with these specification has to be of 100+ order. Unlike [2], completely block the respiration signal is avoided since respiration's 3rd harmonic is extremely close to the heart signal and has comparable power.

The filtered signal at DC can be expressed in vector form of length L samples as,

$$\boldsymbol{r} \approx (\alpha_b D_b) \cdot \boldsymbol{s} + \boldsymbol{z} \tag{31}$$

Where, $\boldsymbol{r} = [r[0] \quad \cdots \quad r[k] \quad \cdots \quad r[L-1]]^T$ is filtered down converted received signal at DC, $D_b = diag[\exp(j\theta_b[0]) \quad \cdots \quad \exp(j\theta_b[L-1])]$ is the Doppler shift due to heart and respiration signal, and $\boldsymbol{z}$ is AWGN. The phase noise is treated as the transmitted signal at DC, $\boldsymbol{s} = [\exp(j\Delta\Phi[0]) \quad \cdots \quad \exp(j\Delta\Phi[L-1])]^T$ and is considered it to be approximately equal for all paths. Further, sample covariance of the baseband signal is estimated to extract the heart and respiration rate.

3.1.3 Covariance estimation

The sample covariance matrix R_{rr}, is estimate through a sliding window of length K samples and an overlap of m samples as shown in Figure 22. To suppress the side bands the Blackman-Harrison window is used.

$$R_{rr} = \mathrm{E}[\,\boldsymbol{r} \cdot \boldsymbol{r}^H] - (\mathrm{E}[\boldsymbol{r}] \cdot \mathrm{E}[\boldsymbol{r}]^H) \tag{32}$$
$$\approx |\alpha_c|^2 R_{ss} + |\alpha_h|^2 D_h R_{ss} D_h^H + |\alpha_r|^2 D_r R_{ss} D_r^H + \sigma^2 I$$

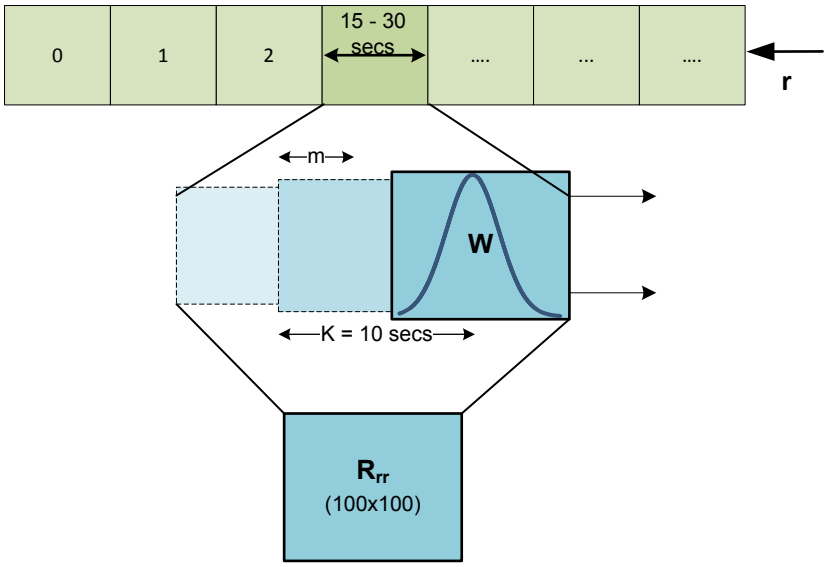

Figure 22: Covariance matrix estimation with sliding window.

Where, R_{ss} is the covariance of the transmitted signal, α_r amplitude of the respiration signal, α_h amplitude of the heart signal, α_c is the residual clutter amplitude after clutter cancellation, D_r is Doppler shift due to respiration, $D_h$is Doppler shift due to heart and σ^2 is AWGN noise power. The windowed signal, $\boldsymbol{r} = W \cdot \left[r[k], \cdots, r[k+K]\right]^T$ where W is a Blackman-Harrison windowing diagonal matrix.

Covariance matrix is generated using a window length of 10 seconds worth of samples to attain a resolution of 0.1Hz with an overlap of greater or equal to 75% over adjacent windows. Minimum of 15 to 30 seconds worth of data is required to reliably estimate the covariance matrix which is further used in PSNS to estimate the heart and respiration rate. The ability to estimate heart rate over 15 to 30 seconds is useful to study the variability of the heart rate which is an important indicator to many cardiovascular diseases [31], [32].

3.1.4 Multiple Signal Classification (MUSIC)

The received signal has closely spaced frequencies primarily due to phase noise skirts of respiration and its harmonics. A simple windowed Fourier transform cannot resolve the

closely space frequencies as seen from Figure 17. MUSIC algorithm is well suited for such a problem [33] and was also adopted in [3] for through wall life detection. MUSIC algorithm belongs to the class of Noise Subspace frequency estimation methods. Noise subspace frequency estimation methods are based on the property that the noise subspace eigenvectors of a Toeplitz autocorrelation matrix are orthogonal to the signal vector. Pisarenko harmonic decomposition (PHD) was the earliest application of this property, although it does not provide reliable estimate itself, it gave way to eigen-analysis for frequency estimation.

The theoretical autocorrelation matrix R_{rr} has following properties, which are exploited by noise subspace frequency estimation methods:

- Autocorrelation matrix R_{rr} is composed of signal auto correlation matrix and noise auto correlation matrix as shown in (32).
- Signal auto correlation matrix is not full rank for $K > p$. p is the number of sinusoids present in the signal of interest.
- The p principal eigenvectors (i.e. eigenvectors corresponding to the p largest eigenvalue) of R_{rr} are identical to that of the signal autocorrelation matrix.
- The p principal eigenvectors $\{\boldsymbol{v}_1 \quad \boldsymbol{v}_2 \quad \cdots \quad \boldsymbol{v}_p\}$ span the signal subspace and the rest span the noise subspace and they are orthogonal to each other.

Eigen decomposition of R_{rr} produces,

$$R_{rr} = \sum_{i=1}^{p} (\lambda_i + \sigma^2)\boldsymbol{v}_i\boldsymbol{v}_i^H + \sum_{i=p+1}^{K} \sigma^2\boldsymbol{v}_i\boldsymbol{v}_i^H \tag{33}$$

where the signal autocorrelation matrix $(|\alpha_c|^2 R_{ss} + |\alpha_h|^2 D_h R_{ss} D_h^H + |\alpha_r|^2 D_r R_{ss} D_r^H)$ is replaced by its Eigen-decomposition $\sum_{i=1}^{p} \lambda_i \boldsymbol{v}_i \boldsymbol{v}_i^H$ and the decomposition of $\sigma^2 I$ is used. Moreover, the principal eigenvectors $\{\boldsymbol{v}_1 \quad \boldsymbol{v}_2 \quad \cdots \quad \boldsymbol{v}_p\}$ span the same subspace as the sinusoids composing the signal $\{e(f_1), e(f_2), \ldots, e(f_p)\}$, where $e(f_i) = \exp(j2\pi f_i k)$. As in our case the signal subspace contains the respiration signal, heart signal and their respective harmonics. If a test tone $e(f_i)$, as illustrated in Figure 23, is scalar multiplied

with eigenvectors of noise subspace and it results in a zero as show in (34), it implies that the test tone belongs to signal subspace as a result of orthogonality. This property of noise subspace is used in MUSIC algorithm to determine the frequency of the sinusoids present.

$$\sum_{\mathrm{j=p+1}}^{\mathrm{K}} \left|\boldsymbol{e}(f_i)^{\mathrm{H}} \cdot \mathbf{v}_{\mathrm{j}}\right| = 0 \tag{34}$$

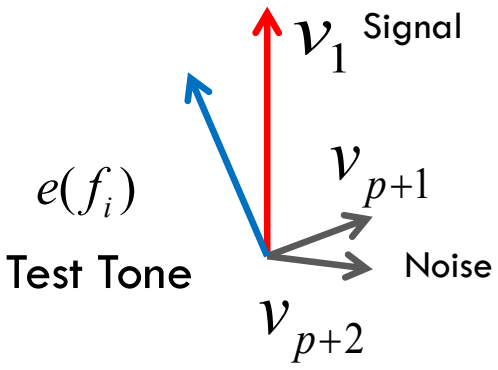

Figure 23: Subspace illustrations

MUSIC algorithm is as follows:

1. Performs Eigen-decomposition of the received signal covariance matrix R_{rr}.
2. The p principal eigenvectors define the signal subspace and the rest define the noise subspace.
3. p is the known or speculated number of sinusoids present in the signal.
4. The sinusoidal frequencies are estimated as the peaks of $P(f)_{MUSIC}$,

$$P(f)_{MUSIC} = \frac{1}{\sum_{i=p+1}^{K} |\boldsymbol{e}(f)^H \cdot \boldsymbol{v}_i|^2} \tag{35}$$

Here $e(f) = \exp(j2\pi fk)$is a test tone and $\boldsymbol{v}_i$ is the ith eigenvector from noise subspace. Theoretically, if the test tone at frequency f belongs to the signal subspace $(f)_{MUSIC} \rightarrow \infty$ due to orthogonality but, due to estimation error in R_{rr} a peaks is produced at the sinusoidal frequency.

3.1.5 Pattern Search in Noise Subspace (PSNS)

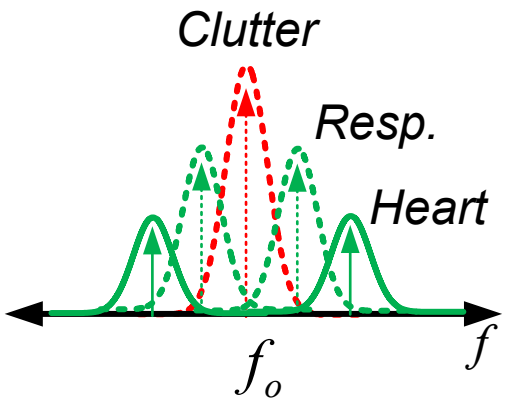

Figure 24 Received signal power spectrum

PSNS is a modified MUSIC algorithm which uses the knowledge of the phase noise of the transmitted signal to detect Doppler shift and hence termed it as Pattern Search in Noise Subspace (PSNS). The inspiration comes from (32) and Figure 24 which clearly suggest that the phase noise covariance R_{ss} is frequency shifted in the received signal. Therefore, instead of searching for generic sinusoids which are orthogonal to the noise subspace as in MUSIC, principal components of R_{ss} should be searched.

PSNS algorithm is as follows:

1. Performs Eigen-decomposition of the received signal covariance matrix R_{rr}, estimated using a windowing function.
2. Create transmit signal vector, $\boldsymbol{s}_{pc}$ using the principal components of R_{ss}
3. The p principal eigenvectors define the signal subspace and the rest define the noise sub-space.
4. The sinusoidal frequencies are estimated as the peaks of $P(f)$,

$$P(f) = \frac{1}{\sum_{i=p+1}^{K} \left| \left(D(f) \cdot \boldsymbol{s}_{pc}\right)^H \cdot \boldsymbol{v}_i \right|^2} \quad (36)$$

Here, $8 \leq p \leq 10$ is the number of Doppler shifts present i.e. the dimension of the signal subspace, v_i is the ith eigenvector of covariance matrix R_{rr} and

$D(f) = diag[\exp(j0) \quad \cdots \quad \exp(j2\pi fk) \quad \cdots \quad \exp(j2\pi fK)]$. $\boldsymbol{s}_{pc}$ is transmit signal vector created using the principal components of phase noise covariance matrix R_{ss} and is expressed as,

$$\boldsymbol{s}_{pc} = \sum_{j=1}^{m} \lambda_j^s \cdot \boldsymbol{v}_j^s \tag{37}$$

Where, λ_j^s and v_j^s are principal eigenvalues and eigenvectors of phase noise signal $s[k]$. The transmitted phase noise is captured through a loopback test i.e. reflected signal is measured once without the person.

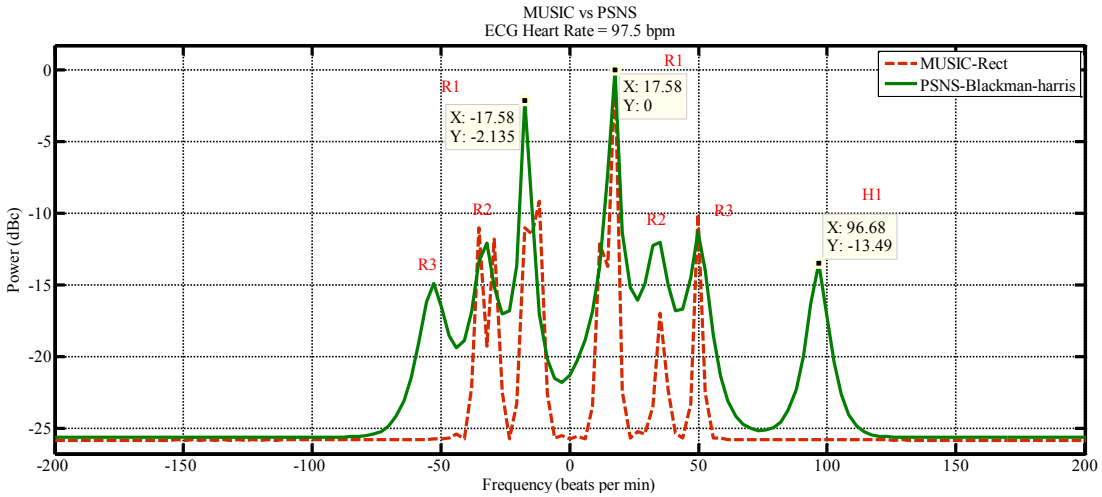

Figure 25: MUSIC vs. PNSN comparison.

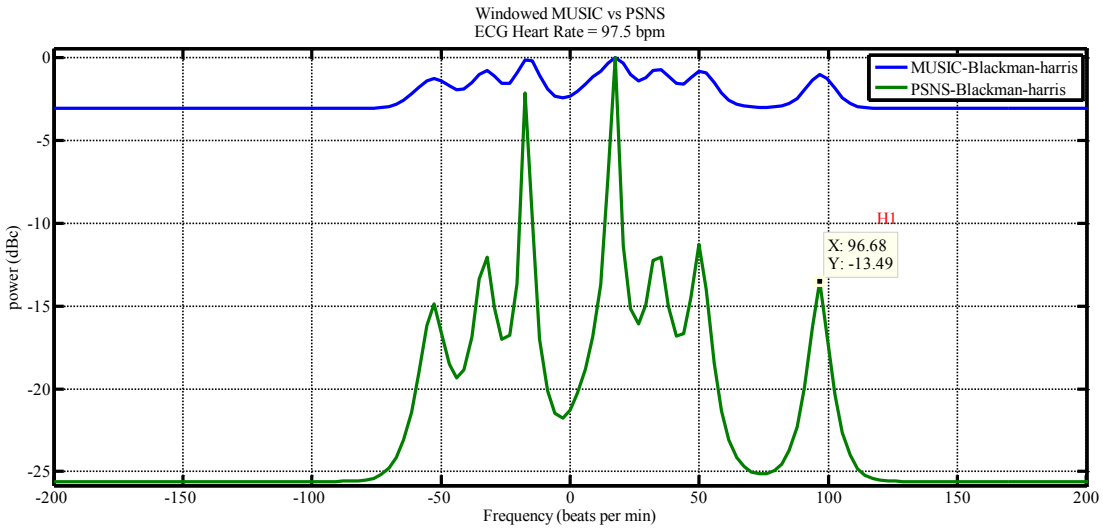

Figure 26: A comparison between MUSIC and PSNS with BH window.

Based on the window chosen for covariance matrix estimation the side bands in PSNS algorithm are suppressed and also helps in pulling out Doppler shifts which are not seen in MUSIC algorithm as seen from Figure 25. In fact, MUSIC algorithm with any window other than rectangular window smears out losing its resolution for spectrum estimation and also pseudo-power of each peak as illustrated in Figure 26.

CHAPTER 4
EXPERIMENTAL SETUP AND SIMULATION MODEL

To effectively understand the problem and its challenges a prototype Doppler radar was implemented using off-the-shelf RF evaluation boards and measurements were made using a 24bit NI ADC. The system was kept as simplistic as possible and was designed as per the proposed architecture. The schematic of the prototype system using the EVM boards is shown in Figure 27. The Clutter cancellation module was left out due to the requirement of a real time system, rather a high resolution ADC was used enabling off-line signal processing and fast prototyping. The Clutter cancellation module was studied through simulation model using both real and simulated data. The goal of prototype is to understand the practical challenges involved in the analog and algorithm design of the system, which would aid in designing a custom low cost integrated solution and signal processing algorithms to extract the vital signs. The learning from the prototype setup and its measurement were also used to come up with a Simulink model to carry out accurate design and testing. The hardware and Simulink models are discussed in the flowing sections.

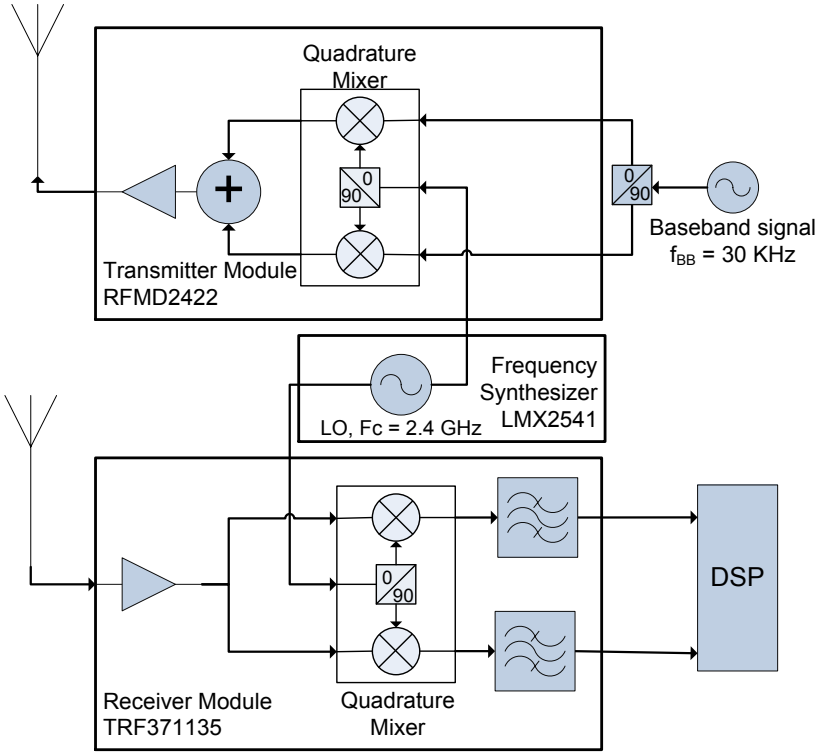

Figure 27: Prototype hardware schematic

4.1 Hardware

The quadrature transmitter selected for prototyping is RFMD 2422 module which has an operating frequency of 800 to 2500 MHz with RF output power up to 3dBm which is sufficient for our application. The quadrature receiver module selected was TI's TRF371135 which has integrated programmable baseband filter and programmable gain amplifiers. TI's LMX2541 low noise frequency synthesizer with integrated VCO is used as an RF source to generate the 2.38 GHz signal. As shown in Figure 27 the transmitter module is driven by a signal generator at baseband which produces the quadrature IF signal at 30 KHz. On the receiving end the RF signal is amplified through am ultra-low noise amplifier (LNA) RFMD SPF-5122Z and the baseband I/Q signal from the receiver module is fed to NI DAQ 5922. Yagi-Uda antennas pair with 9dBi gain and 60° beam width is used for transmission and reception of EM waves. The antenna gain pattern is

show in Figure 29. These directional antennas were chosen to provide maximum Tx-Rx isolation of about 50dB as well as reduce clutter by limiting the view field of the antenna.

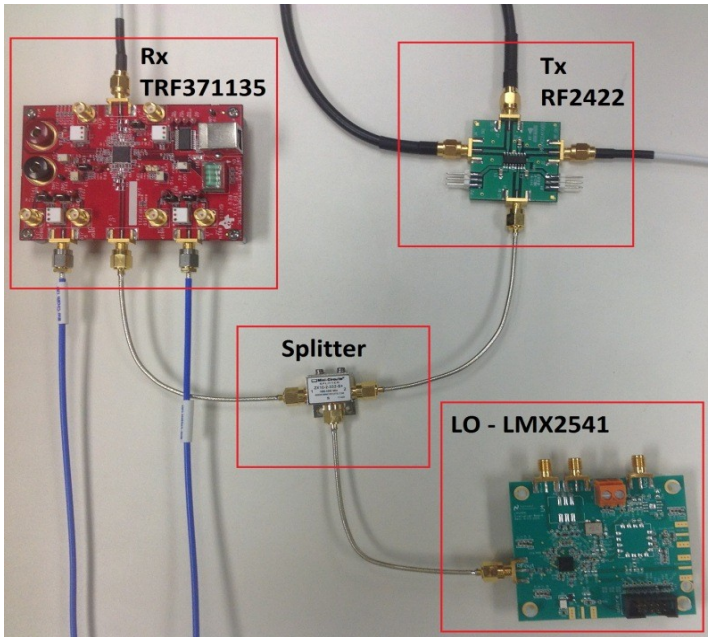

Figure 28: Prototype hardware setup using off-the-shelf evaluation boards

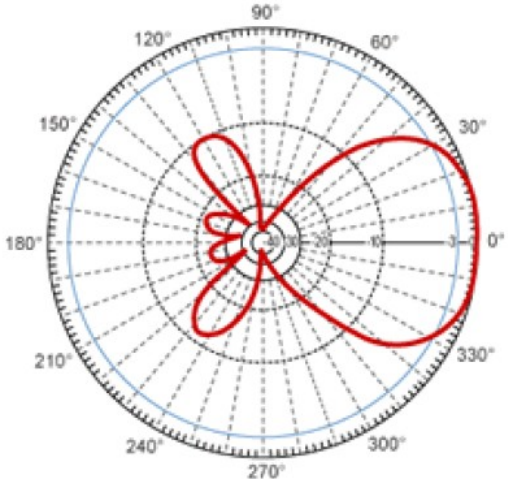

Figure 29: Antenna gain pattern of Yagi-Uda antenna

The transmitted baseband signal $s(t)$ has an IF = 30 KHz, as it can be seen from its power spectrum in Figure 30. Intermediate frequency of 30KHz is chosen as it is the corner frequency of the receiver TRF371135 where $\frac{1}{f}$ noise and thermal noise are equal which can be observed from Figure 35. This baseband signal $s(t)$ is quadrature mixed by RFMD 2422 with the LO signal at 2.38GHz to obtain RF signal $S(t)$ at $2.380\ GHz + 30\ KHz$. The power spectrum of LO signal is show in Figure 31 and that of the resultant transmission signal in Figure 32.

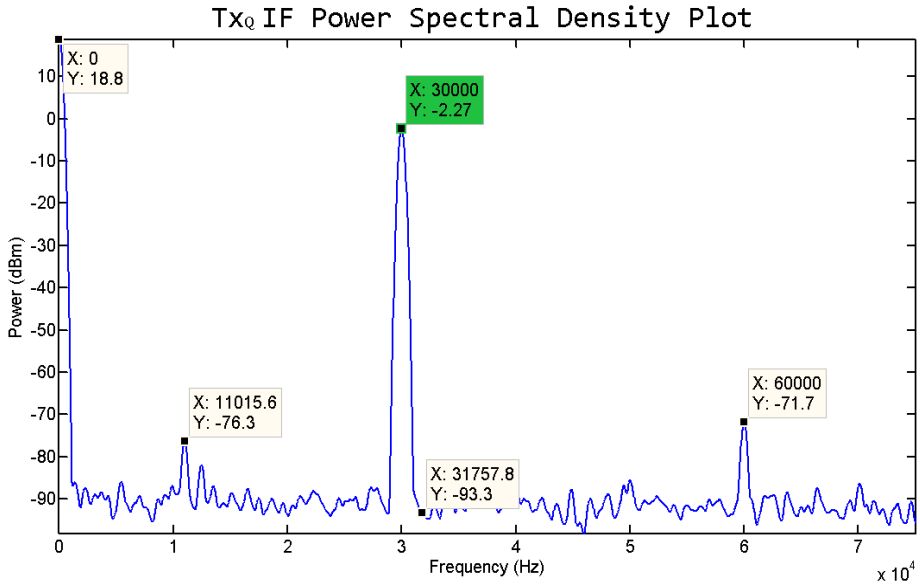

Figure 30: Power spectrum of the baseband transmit signal, I/Q-channel.

The upper sideband can be seen to dominate while the carrier and the lower sideband are suppressed by 34dB and 41dB respectively in comparison to upper sideband. The transmission signal with -12.9 dBm power is transmitted through the Yagi antenna. These measurements were carried out in an anechoic chamber hence the received signal is nothing but the Tx-Rx leakage. Figure 33 illustrates the power spectrum at the receiving antenna and one can conclude that the isolation here between Tx-Rx paths is 42dB. The received RF signal is amplified by the LNA which amplifies the signal by 9dB and has a noise figure of 0.86 dB. The power spectrum of the output of LNA can be seen in Figure 34. This signal is used for down-conversion to baseband signal by mixing the

signal with the LO signal. The resulting baseband signal power spectrum is shown in Figure 35 and Figure 36. This signal is amplified and digitized using NI-DAQ and the respiration and heart beat is estimated as explained in Chapter 3.

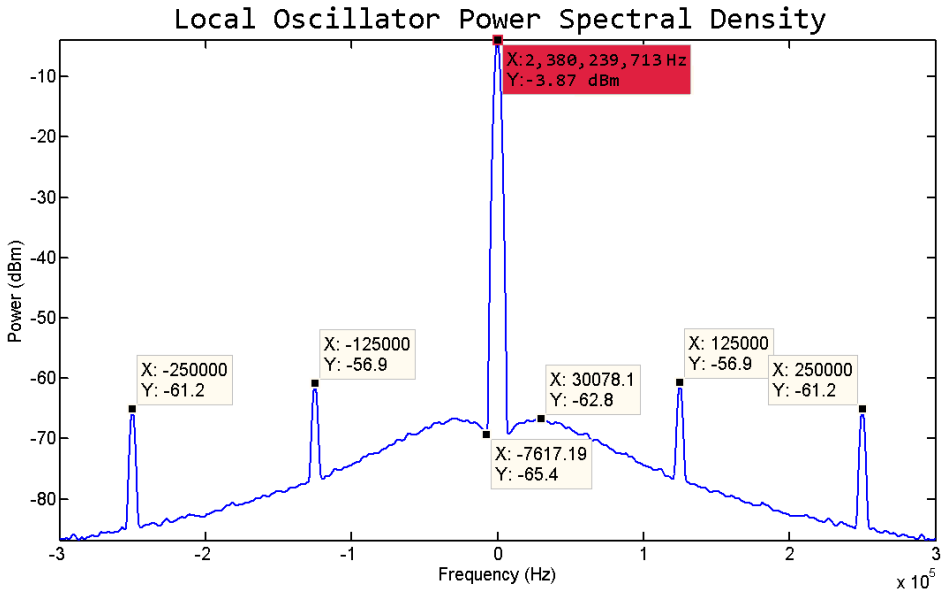

Figure 31: Power Spectrum of LO LMX 2541 at 2.380 GHz

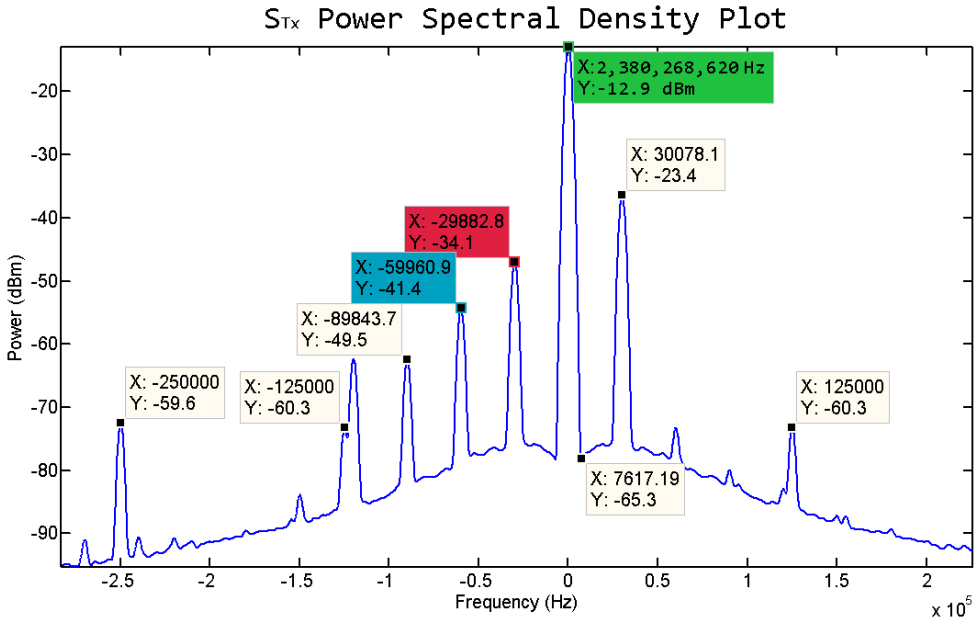

Figure 32: Power spectrum of the mixed signal at the output of the RFMD 2422.

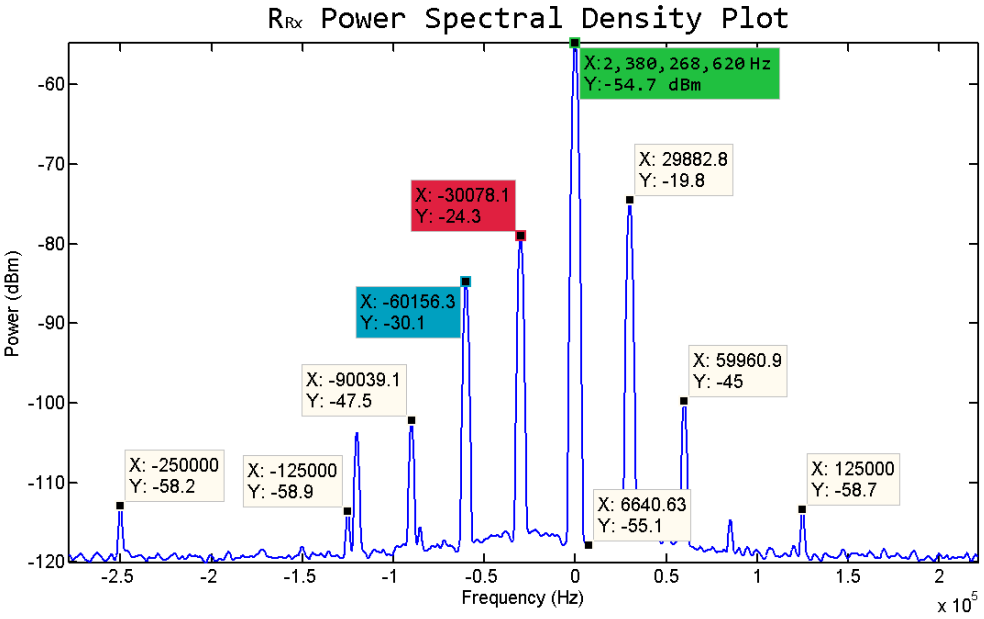

Figure 33: Power spectrum of received signal at the antenna.

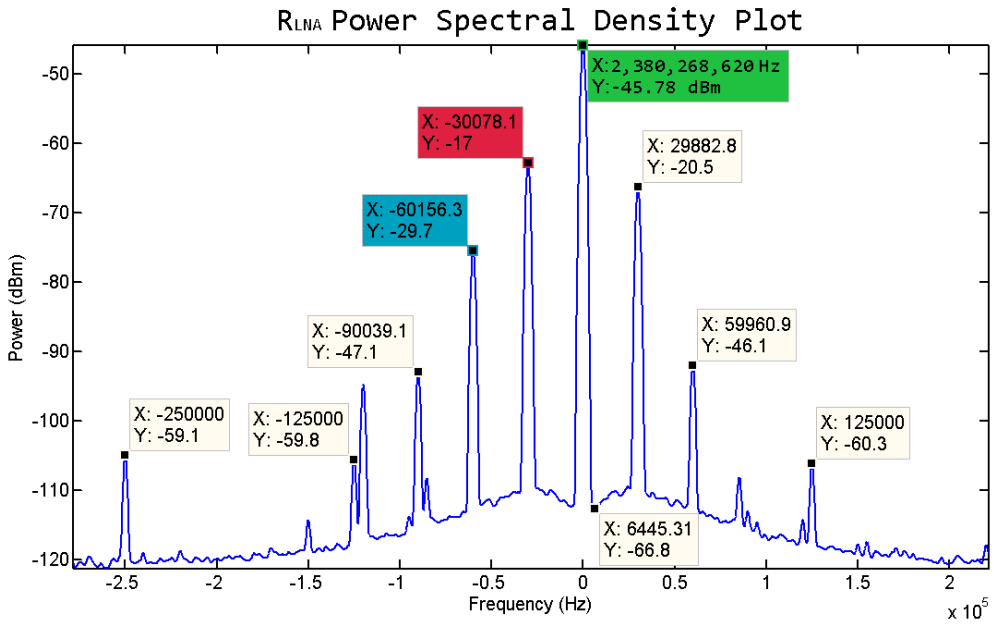

Figure 34: Power spectrum of LNA output.

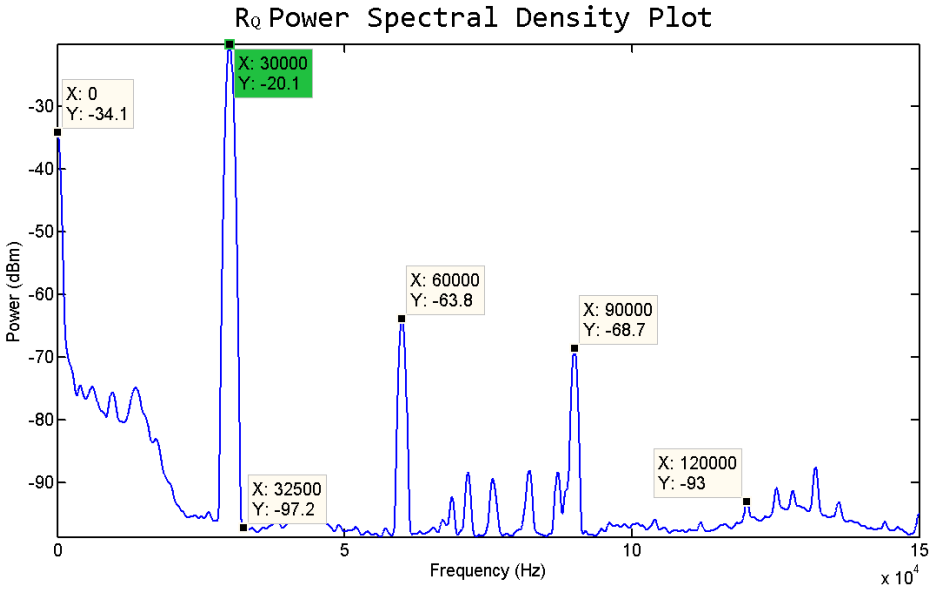

Figure 35: Power spectrum of received baseband signal, Q-channel

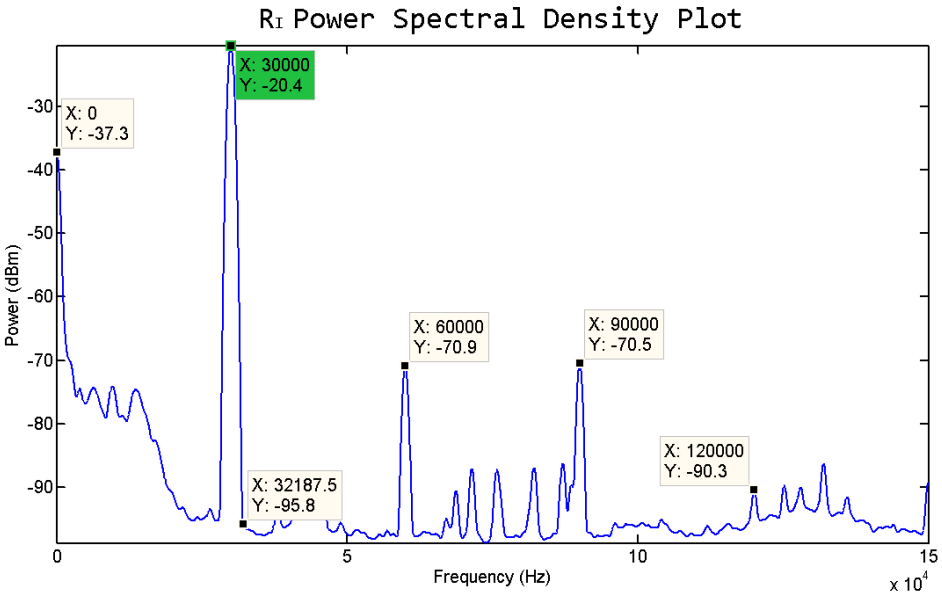

Figure 36: Power spectrum of received baseband signal, I-channel

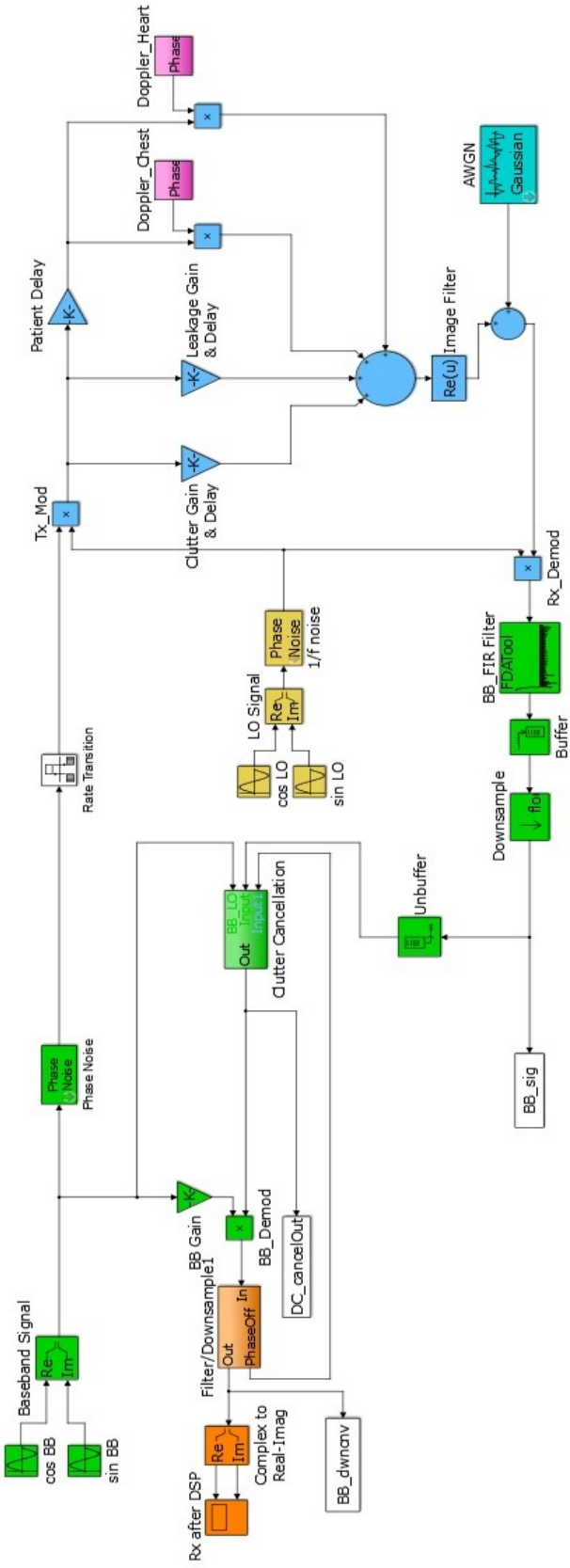

Figure 37: Simulink model

4.2 Simulation Model

Utilizing the understanding of the heart and respiration signal drawn from the measurements made from the prototype system an equivalent channel model of heart, chest and clutter was developed in Simulink as illustrated in Figure 37. The heart and chest are modeled as sinusoidal oscillations at heart and respiration rate respectively as expressed in (11). The dominant noise source, the phase noise was included by mimicking the phase noise characteristics of the LMX-2541 through the Simulink phase noise RF block. This also aids in studying the effect of Range correlation on measurements. Figure 38 shows the received signal at baseband with respiration rate of 20 BPM (0.3Hz) and heart rate of 72 BPM (1.2 Hz).

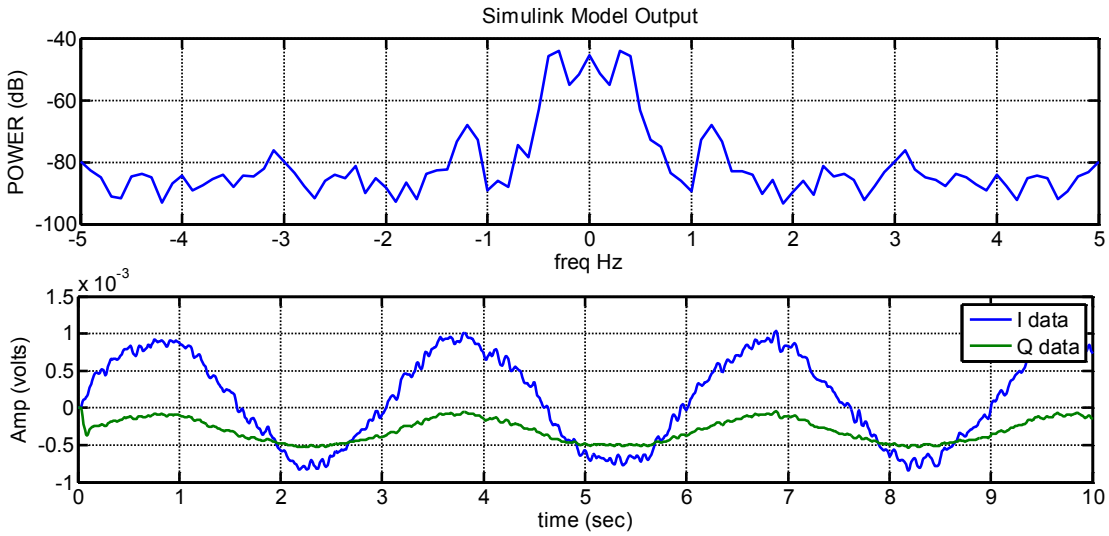

Figure 38: Respiration at and heart beat simulation

4.3 Measurements

To validate the architecture and algorithms employed multiple measurement were made over eight adult volunteers (4 males, 4 females) over different distance. They were asked to sit still on a chair in a room with their chest facing the Doppler radar as shown in Figure 2 and breathe in a relaxed manner. The distance of the person from the antenna was varied from 1m to 6m and measurement was recorded for 60 seconds. Three lead ECG was used as a reference to validate the heart rate. Table 1 contains the weight, height and BMI of each subject and Table 2 contains

their respective heart rates estimate, using the Doppler radar at 1 and 3m distance, compared with ECG. Resultant average error is ±3.29 BPM with a standard deviation of ±4.03 BPM.

Table 1: Measured data of volunteers

Subject	Gender	Age (yrs)	Weight (Kg)	Height (m)	BMI (Kg/m^2)
M1	M	26	65.00	1.88	18.40
M2	M	28	54.43	1.70	18.79
M3	M	23	78.93	1.70	27.25
M4	M	28	87.00	1.80	26.85
F1	F	29	58.97	1.75	19.20
F2	F	48	68.04	1.73	22.81
F3	F	20	68.04	1.70	23.49
F4	F	21	72.57	1.65	26.63
Mean		**27.88**	**69.12**	**1.74**	**22.93**
Stdev		**±8.81**	**±10.46**	**±0.07**	**±3.77**

Table 2: ECG vs. Doppler radar (DR) heart rate estimate

	Distance 1m			Distance 3m		
Subject	ECG (BPM)	DR Est. (BPM)	Err (BPM)	ECG (BPM)	DR Est. (BPM)	Err (BPM)
M1	106	101	5	98.5	96.7	1.8
M2	94.5	95	0.5	97	87	10
M3	79.5	78.5	1	79	78.5	0.5
M4	109.5	109	0.5	107.5	107.2	0.3
F1	96	102	6	98	96	2
F2	64.5	66	1.5	65	77	12
F3	69.5	68.5	1	68.5	68.5	0
F4	58	57.42	0.58	56	66	10

4.4 Respiration Harmonics

As mentioned earlier the harmonics of respiration make the detection problem extremely challenging when they fall close to the heart signal. It can be clearly be seen in Figure 39 where 2nd respiration harmonic R3 is extremely close to the heart signal H1. To differentiate between extremely close heart and respiration harmonic spectrum has to be estimated over a large duration. Since heart and respiration are not stationary signal their frequencies vary over time hence spectrum estimation over large duration is futile. Hence spectrum estimation over smaller duration with PSNS algorithm is helpful. Here 15 seconds of the total 60 seconds of data was used to estimate the spectrum. Also in Figure 39 we also see the second harmonic of the heart H2 this can be used to differentiate between heart signal and respiration harmonic as they are not exact integer multiples.

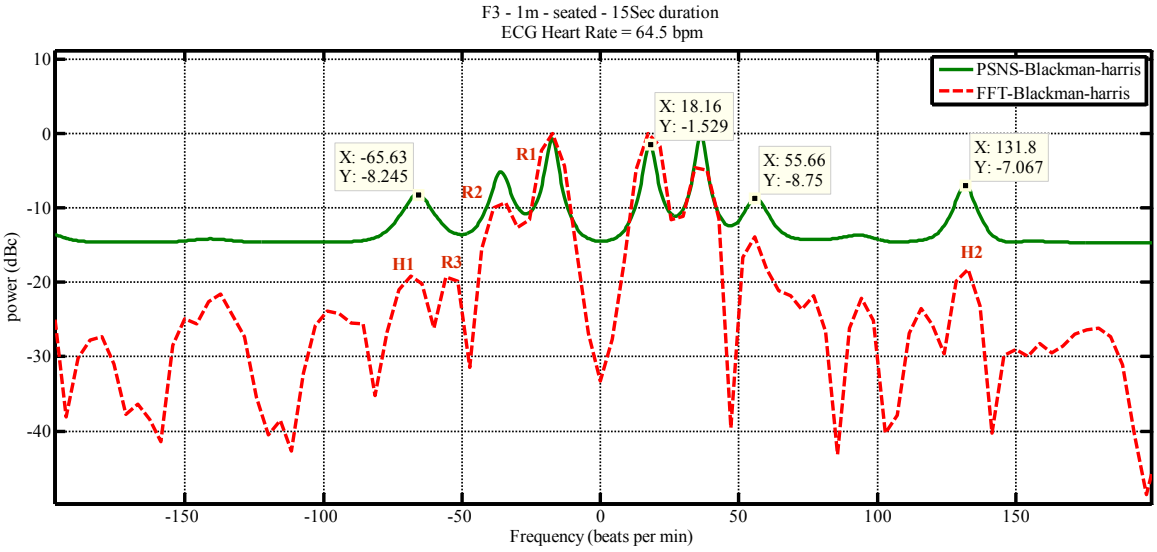

Figure 39: Spectrum analysis of 20 seconds of data from subject F3's.

4.5 Heart Variability

The heart rate is known to vary over time which is a sign of healthy heart [32]. The variability of the heart is used as an indicator of the heart health. But this variability makes the detection difficult hence we must estimate the signal over a period where the heart rate is relatively stationary. In Figure 40 we can see how the variability of the heart over 60 seconds adds multiple

peaks to the spectrum estimation and PSNS fails to record a clear single peak of heart beat. Hence the duration over which the heart rate is estimated needs to be small but large enough to have an acceptable covariance matrix with maximum delay of 10secs as required to have 6 beat per minute resolution. We observed covariance when estimated over min 15-20 seconds proved to be sufficient with 95% overlap between windows to estimate covariance as discussed in Section 3.1.3.

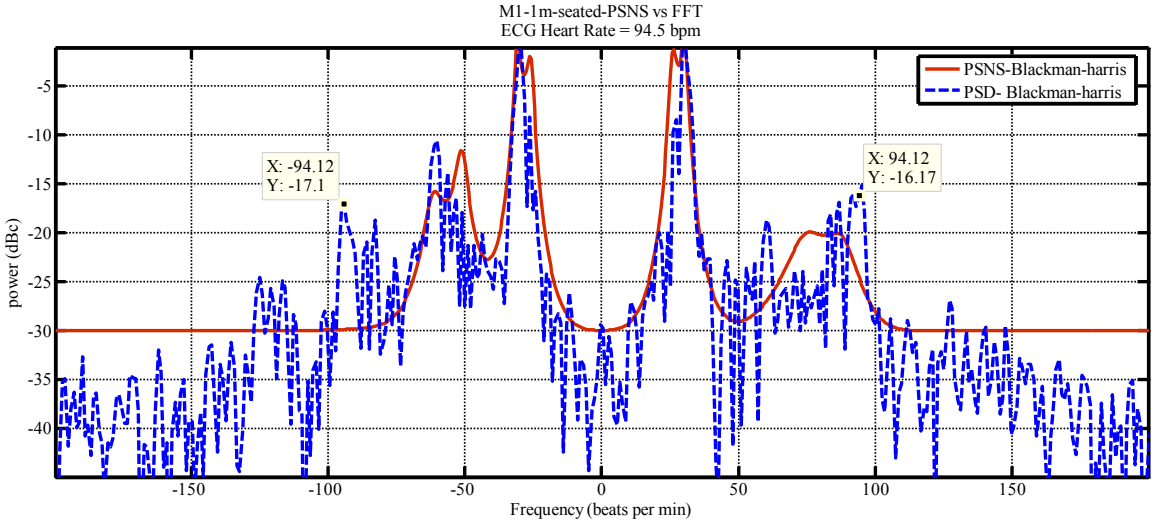

Figure 40: Spectrum estimate over 60secs of measurement of subject M1.

The heart beat was estimated over 20 second data rather than the complete 60 seconds of data. We can observe that the heart rate varies from 104 to 94 beats per min over a minute in Figure 41.

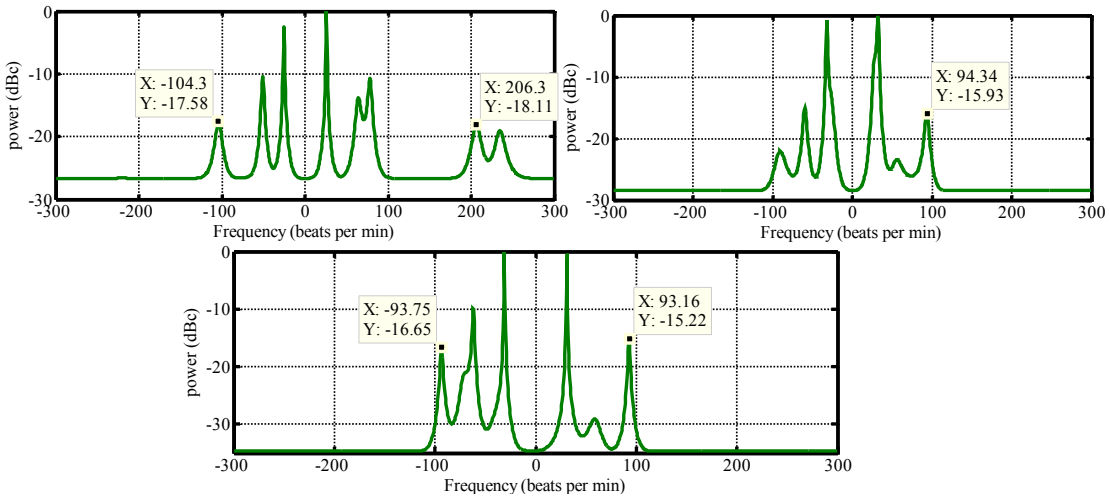

Figure 41: Heart beat estimate over 20 seconds of subject M1 seated at 1m.

Chapter 5
CONCLUSIONS

Vital sign monitoring through Doppler radar provides a method to accurately estimate respiration and heart rate of a relatively still subject without contact and through their clothing. The instrument was developed from readily and cheaply available RF ICs and demonstrated the ability to measure heart and respiration rate up to 6m in presence of strong clutter. These capabilities were achieved through the analog architecture and signal processing algorithms which have been discussed in prior chapters. This instrument could greatly help in application where contact is to be avoided such as skin burn patience and neonates or in search and rescue operations to detect life below debris. The system was tested for eight subjects over multiple distances and their heart and respiration rate were accurately estimated.

5.1 Future Work

For the Doppler radar to be versatile and usable in daily life signal processing has to be greatly improved. Especially in detection of multiple subjects and cancellation of body motion so that vital sign can be estimated in any posture or act. Using multiple transceivers with MIMO signal processing could be used for detecting vital signs of multiple users [12] and also for isolation body motion from vital signs.

5.1.1 Body motion cancellation

Random human body motion and the natural fidgeting distorts the Doppler signal significantly, making extraction of vital sign make extremely difficult. Since body motion is random and irregular, suppressing too is challenging.

Two transceivers placed front and behind of a person under observation to cancel random body has been suggested by Li et al [13]. The fact that the heart and respiration are more prominent on the chest wall compared to the back where as the body motion is comparable from both sides is used to cancel body motion. But this requires unobstructed view of the person from both sides and the motion from both sides is not always symmetric.

Differential front end approach for cancelling body motion has been suggest in [15]. Here two helical antennas are used to illuminate the chest and the abdomen. The notion here is that one beam detects the body motion and the vital sign while the other only picks up body motion, subtracting these two signals results in respiration and heart signal. The disadvantage here is that it can only cancel subtle body motion while the subject is standing still but not large motions like moving of hands or legs.

A single transceiver solution is more attractive which can cancel all body motions which could be achieved by using multiple microwave frequencies. The body motion due to vital sign is in the order of millimeters, small wavelength frequencies are more sensitive to these minute motions where as large wavelength frequencies are only sensitive to large motion. Hence by subtracting the received signal across different frequencies could help in cancelling random body motion using just one transceiver which emits multiple radio frequencies.

5.2 Summary

Doppler Radar based vital sign monitoring can greatly benefit our society as it offers a promising noncontact instrument to measure vital signs through clothing or obstruction. An integrated solution would make the technology inexpensive and make it available to the masses through household products. Further advances in signal processing could make the instrument more versatile and broaden its applications.

REFERENCES

[1] J. C. Lin, "Noninvasive Microwave Measurement of Respiration," in *Proceedings of the IEEE*, 1975, vol. M, no. October, p. 1530.

[2] A. D. Droitcour, "Non-Contact Measurment of Heart and Respiration Rates with a Single-Chip Microwave Doppler Radar," Stanford, 2006.

[3] M. Ascione, A. Buonanno, M. D. Urso, and L. Angrisani, "A New Measurement Method Based on Music Algorithm for Through-the-Wall Detection of Life Signs," *IEEE Transactions on Instrumentation and Measurement*, pp. 1–14, 2012.

[4] A. Norman, C. Kun-Mu, Y. Huang, and J. Zhang, "Microwave Life-Detection Systems for Searching Human Subjects Under Earthquake Rubble or Behind Barrier," *IEEE Transactions on Biomedical Engineering*, vol. 27, no. 1, pp. 105–114, 2000.

[5] M. Singh and G. Ramachandran, "Reconstruction of sequential cardiac in-plane displacement patterns on the chest wall by laser speckle interferometry.," *IEEE transactions on bio-medical engineering*, vol. 38, no. 5, pp. 483–9, May 1991.

[6] D. R. Morgan and M. G. Zierdt, "Novel signal processing techniques for Doppler radar cardiopulmonary sensing," *Signal Processing*, vol. 89, no. 1, pp. 45–66, Jan. 2009.

[7] M. Chen, O. Boric-lubecke, and V. M. Lubecke, "0.5- μm CMOS Implementation of Analog Heart-Rate Extraction With a Robust Peak Detector," *IEEE Transactions on Instrumentation and Measurement*, vol. 57, no. 4, pp. 690–698, 2008.

[8] I. Mostafanezhad, O. Boric-Lubecke, and V. Lubecke, "A coherent low IF receiver architecture for Doppler radar motion detector used in life signs monitoring," *2010 IEEE Radio and Wireless Symposium (RWS)*, no. 1, pp. 571–574, Jan. 2010.

[9] F. Wang, S. Member, T. Horng, S. Member, K. Peng, and J. Jau, "Detection of Concealed Individuals Based on Their Vital Signs by Using a See-Through-Wall Imaging System With a Self-Injection-Locked Radar," vol. 61, no. 1, pp. 696–704, 2013.

[10] C. Li, V. M. Lubecke, S. Member, O. Boric-lubecke, and J. Lin, "A Review on Recent Advances in Doppler Radar Sensors for Noncontact Healthcare Monitoring," vol. 61, no. 5, pp. 2046–2060, 2013.

[11] Q. Zhou, J. Liu, A. Høst-madsen, O. Boric-lubecke, and V. Lubecke, "Detection of multiple heartbeats using doppler radar †," pp. 1160–1163, 2006.

[12] D. Samardzija, O. Boric-Lubecke, A. Host-Madsen, V. M. Lubecke, T. Sizer, A. D. Droitcour, and G. T. A. Kovacs, "Applications of MIMO Techniques to Sensing of

Cardiopulmonary Activity," *IEEE/ACES International Conference on Wireless Communications and Applied Computational Electromagnetics, 2005.*, pp. 618–621.

[13] C. Li and J. Lin, "Random Body Movement Cancellation in Doppler Radar Vital Sign Detection," *IEEE Transactions on Microwave Theory and Techniques*, vol. 56, no. 12, pp. 3143–3152, Dec. 2008.

[14] X. Yu, C. Li, and J. Lin, "Two-dimensional noncontact vital sign detection using Doppler radar array approach," *2011 IEEE MTT-S International Microwave Symposium*, pp. 1–4, Jun. 2011.

[15] R. Fletcher, "Low-cost differential front-end for Doppler radar vital sign monitoring," *2009 IEEE MTT-S International Microwave Symposium Digest*, pp. 1325–1328, Jun. 2009.

[16] A. D. Droitcour, S. Member, O. Boric-lubecke, S. Member, V. M. Lubecke, J. Lin, G. T. A. Kovacs, and A. D. Doppler-radar, "Range Correlation and I/Q Performance Benefits in Single-Chip Silicon Doppler Radars for Noncontact Cardiopulmonary Monitoring," vol. 52, no. 3, pp. 838–848, 2004.

[17] I. Mostafanezhad and O. Boric-lubecke, "An RF Based Analog Linear Demodulator," *IEEE Microwave and Wireless Components Letters*, vol. 21, no. 7, pp. 392–394, 2011.

[18] D. Girbau, A. Lázaro, Á. Ramos, and R. Villarino, "Remote Sensing of Vital Signs Using a Doppler Radar and Diversity to Overcome Null Detection," *IEEE Sensors*, vol. 12, no. 3, pp. 512–518, 2012.

[19] B. Park, S. Member, O. Boric-lubecke, S. Member, and V. M. Lubecke, "Arctangent Demodulation With DC Offset Compensation in Quadrature Doppler Radar Receiver Systems," vol. 55, no. 5, pp. 1073–1079, 2007.

[20] O. B. Lohman, Boric-Lubecke, V. M. Lubecke, P. W. Ong, and M. M. Sondhi, "A digital signal processor for Doppler radar sensing of vital signs.," *IEEE engineering in medicine and biology magazine : the quarterly magazine of the Engineering in Medicine & Biology Society*, vol. 21, no. 5, pp. 161–4, 2002.

[21] C. Gu, C. Li, and J. Lin, "Instrument-Based Noncontact Doppler Radar Vital Sign Detection System Using Heterodyne Digital Quadrature Demodulation Architecture," *IEEE Transactions on Instrumentation and Measurement*, vol. 59, no. 6, pp. 1580–1588, 2010.

[22] Ø. Aardal, Y. Paichard, S. Brovoll, T. Berger, T. S. Lande, and S.-E. Hamran, "Physical working principles of medical radar.," *IEEE transactions on bio-medical engineering*, vol. 60, no. 4, pp. 1142–9, Apr. 2013.

[23] M. C. Budge and M. P. Burt, “Range correlation effects on phase and amplitude noise,” *Proceedings of Southeastcon ’93*, p. 5, 1993.

[24] A. D. Droitcour, O. Boric-lubecke, and G. T. A. Kovacs, “Signal-to-Noise Ratio in Doppler Radar System for Heart and Respiratory Rate Measurements,” *IEEE Transactions on Microwave Theory and Techniques*, vol. 57, no. 10, pp. 2498–2507, 2009.

[25] V. M. Lubecke, O. Boric-Lubecke, A. Host-Madsen, and A. E. Fathy, “Through-the-Wall Radar Life Detection and Monitoring,” *2007 IEEE/MTT-S International Microwave Symposium*, pp. 769–772, Jun. 2007.

[26] I. Mostafanezhad, O. Boric-Lubecke, V. Lubecke, and A. Host-Madsen, “Cancellation of unwanted motion in a handheld Doppler radar used for non-contact life sign monitoring,” *2008 IEEE MTT-S International Microwave Symposium Digest*, no. 3, pp. 1171–1174, Jun. 2008.

[27] D. W. Lin, “Echo Cancellation Algorithms,” no. April, 1984.

[28] M. Sondhi, “An self-adaptive Echo Canceller.” Bell Labs.

[29] S. L. Gay and B. Labs, “An Efficient, Fast Converging Adaptive Filter for Network Echo Cancellation,” pp. 394–398, 1998.

[30] B. Razavi, “A 125-MHz mixed-signal echo canceller for Gigabit Ethernet on copper wire,” *IEEE Journal of Solid-State Circuits*, vol. 36, no. 3, pp. 366–373, Mar. 2001.

[31] U. Rajendra Acharya, K. Paul Joseph, N. Kannathal, C. M. Lim, and J. S. Suri, “Heart rate variability: a review.,” *Medical & biological engineering & computing*, vol. 44, no. 12, pp. 1031–51, Dec. 2006.

[32] H. M. Stauss, “Heart rate variability.,” *American journal of physiology. Regulatory, integrative and comparative physiology*, vol. 285, no. 5, pp. R927–31, Nov. 2003.

[33] S. M. Kay and S. L. Marple, “Spectrum Analysis-A Modern Perspective,” *Proceedings of the IEEE*, vol. 69, no. 11, pp. 1380–1419, 1981.